Dynamic response of an infinite beam periodically supported by sleepers resting on a regular and infinite lattice

Semi-analytical solution

de Oliveira Barbosa, João Manuel; van Dalen, Karel N.

DOI
10.1016/j.jsv.2019.06.014

Publication date
2019

Document Version
Accepted author manuscript

Published in
Journal of Sound and Vibration

Dynamic response of an infinite beam periodically supported by sleepers resting on a regular and infinite lattice: semi-analytical solution

by

João Manuel de Oliveira Barbosa[a*] & Karel N. van Dalen[a]

[a]TU Delft, Faculty of Civil Engineering and Geosciences (CiTG), Department of Engineering Structures, Section of Dynamics of Solids and Structures. Stevinweg 1, 2628 CN Delft, The Netherlands
[*]corresponding author: J.M.DeOliveiraBarbosa@tudelft.nl

Abstract

In this work we propose a model for the analysis of the dynamic behaviour of a ballasted track that combines discrete and continuous elements. The rail is modelled via an Euler-Bernoulli beam, the periodically spaced sleepers are represented with lumped masses, and the ballast is simulated using a lattice (regular network of elastically connected lumped masses). All elements are assumed to behave linearly, and the lattice can be supported by a flexible or a rigid foundation, simulating soil or a hard rock. The equations of motion of each component are presented and the coupled system is solved semi-analytically in the frequency domain. The time domain response can be calculated afterwards by means of a numerical inverse Fourier transform. Dispersion curves and time responses are produced for the case of a ballasted track on a stiff soil. These responses are compared with the scenario in which ballast is modelled as lumped supports, and the scenario in which the force is applied directly to the ballast (no superstructure). It is observed that the simpler models fail to capture the vibration modes in which energy is concentrated in the ballast, and that the superstructure significantly alters the response of the track, increasing its critical velocity and changing the deformed shape of the ballast. The model herein proposed can be used to assess the dynamic characteristics of the track (critical speeds, energy propagation, vehicle-track interaction, etc.) and will serve as framework for a development of a tool for assessment of the settlement behaviour of ballast.

Keywords: periodic structures; moving load; infinite beam; infinite lattice.

1. Introduction

Maintenance work on railway tracks is a substantial part of railway infrastructures budget, it limits the availability of the tracks and contributes significantly to the ticket's fares. A considerable part of the maintenance tasks correspond to the restoration of the vertical position of the track, which changes over time due to soil consolidation and ballast settlement. The issue of differential ballast settlement is more pronounced in zones with variations in the support stiffness, as observed in track-bridge transition zones and track-tunnel transitions [1–4].

In order to propose solutions to reduce the settlement rate of ballast (and in this way, reduce maintenance costs), the mechanisms that drive the ballast settlement must be understood. For that reason, mathematical models that consider the appropriate behaviour of ballast and other track components are desired as they allow assessing how alterations in the track change its response.

That is the motivation for this work, in which a model for ballast (plus sub-grade[1]) and rails is presented.

Physical models focusing on the behaviour of ballast range from simplified linear-continuum models to nonlinear discrete models. Linear models are easier to solve at the expense of obtaining less accurate predictions, while nonlinear models represent the physics more accurately, though they usually require an immense computational effort. Continuum models can be solved using, for example, the finite element method (FEM, which can be linear [5–7] or nonlinear [8,9] – the nonlinear FEM models allow for plasticity and intend to replicate the settlement behaviour), while discrete models are usually solved with discrete element methods (DEM) [10–14]. The method proposed in this work falls into the category of discrete models, as it aims at characterizing the response of each individual particle in the ballast. However, it is assumed that the ballast particles are all equal in size and shape and regularly distributed, and that their 'connectivity' is space invariant. It is expected that this type of model provides more accurate results than models that neglect the discrete character of ballast, and at the same time that it keeps the calculations simpler by avoiding the calculation of contact points between particles (like in DEM, for which the geometry of each individual particle is of relevance).

At this phase, the connection between stones is assumed linear and no longitudinal subgrade stiffness variations are considered. The objective of this work merely is to introduce the model concept and to present the mathematical tools needed to, at a later stage, couple the infinitely long model here proposed to a compatible model with finite length, cast in the space-time domain, and in which nonlinearities and stiffness variations are present. How to couple the model presented here to a finite space-time domain model, and how the introduction of nonlinearities affects the track response will be addressed in follow-up papers.

The model presented in this work is that of an infinite beam periodically supported by sleepers, which in turn rest on a lattice. Beams on periodic supports differ from those on continuous supports [15] in the sense that the transmission of forces to the foundation happens at localized regions instead of continuously along the beam, thus changing the short wavelength (high frequency) bending behaviour of the beam. Models of infinite beams on periodic supports have been presented and handled analytically in the past. These models are solved with Fourier series expansions [16,17], application of the so-called periodicity condition [18,19], or application of the Floquet's theorem [20,21]. The six works mentioned above consider the supports to respond independently of the neighbouring ones (either fixed supports or local elastic connections), but other works have also been published in which the supports are interconnected through an elastic medium [22–24]. The main difference between the model proposed in this work and those proposed in the past resides in the type of medium connecting the supports, which in the present case is discrete and periodic, with periodicity shorter than that of the supports. To the best of the authors' knowledge, it is the first time that a system consisting of a continuum medium (beam) and a foundation with two distinct periodicities (sleepers and lattice) is handled analytically.

[1] In the examples presented in this work, the sub-grade is assumed stiff, but it can be made flexible by considering a layered lattice with distinct properties for ballast and sub-grade. See Appendix I for the definition of layered lattice.

The solution method employed in this work differs from those based on the periodicity condition in the sense that it does not assume such type of response (thus allowing to calculate the response for both moving and non-moving loads) and from those based on Floquet's theory in the sense that the response is not directly based on propagation factors and propagation shapes. Instead, the frequency domain response of each component is written as a spatial convolution of unknown interaction forces and the Green's functions of the components (which are known). The variables to be convolved are transformed to the wavenumber domain (via the Fourier Transform of discrete signals, in some works called Floquet Transform [25]), and from the resulting equations the interaction forces (and subsequently the response of each component) can be readily obtained in the transformed domain. The transformation back to the space domain is achieved via the inverse Fourier transform, which results in an integral over a finite wavenumber region. For the case of moving loads, the integral can be evaluated analytically.

The manuscript is organized as follows. Section 2 describes the model and the solution method. In Section 3, the obtained equations are used to calculate the free vibration modes of the track. In Section 4, the method is verified by comparing the proposed method with a purely numerical one, for the case of loads moving on the beam. In Section 5, the influence of the rails and sleepers on the critical speeds of the system is analysed by comparing the results with those obtained by other authors who considered a similar model but excluded the superstructure [26]. In the last section, Section 6, the work is summarized and final considerations are proffered.

2. Track model

The model proposed in this work builds up on the model presented by Suiker and collaborators [26,27] in the sense that the superstructure (sleepers and the rails) is also considered. It is a two-dimensional model, where rails are simulated with an Euler-Bernoulli beam with bending stiffness EI_{rail} and mass per unit length m_{rail}, sleepers are considered via rigid masses with translational inertia M_{s} and rotational inertia J_{s}, and ballast (and soil) is modelled via a lattice, i.e., an assemblage of rigid masses connected via a regular network of vertical, horizontal and diagonal springs (same as Suiker et al.). Rails are connected to the sleepers via the rail pads, which are simulated via vertical springs of constant K_{v} and rotational springs of constant K_{θ}. Between sleepers and grains of ballast (mass of the lattice network) there are vertical springs of constant K_{usp} that simulate under-sleeper pads. It is assumed that there is no transmission of horizontal forces from the sleepers to the ballast, i.e., there is a frictionless connection between the two parts: in this way, the horizontal motion of the particles at the surface of the ballast is not constrained in any way. Figure 1 shows a schematization of the model.

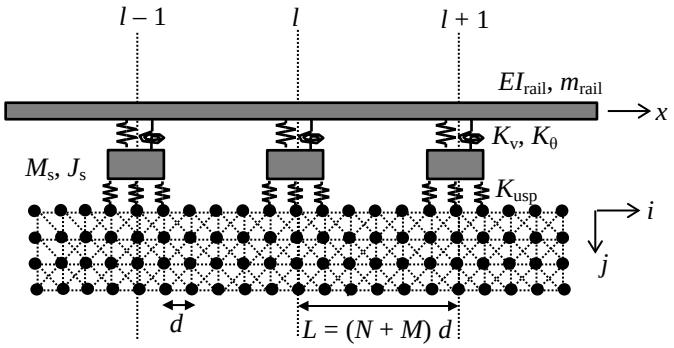

Figure 1. Schematization of the model around the lth sleeper.

It is assumed that the structure repeats itself periodically, never starting nor ending. The contact points between sleepers and ballast are always at the same position relative to the sleeper, and so are the free ballast grains between sleepers. The number of contact points between sleepers and ballast is defined by N, while the number of free grains between sleepers is defined my M. Both are integer numbers. The sleeper distance (and periodicity of the system) is $L=\left(N+M\right)d$, where d is the spacing between the particles of the lattice.

The external forces acting on the structure are distributed forces $F_{\text{ext}}\left(x\right)$ and distributed moments $M_{\text{ext}}\left(x\right)$ on the rail (x is the longitudinal coordinate, and $x=0$ corresponds to the centre of sleeper at reference cell $l=0$), and vertical and horizontal forces $F_{\text{v},e}$ and $F_{\text{h},e}$ acting on ballast particle e situated at column i_e and row j_e of the lattice network ($i=0$ corresponds to the leftmost particle connected to sleeper $l=0$; $j=0$ corresponds to the upper surface of the ballast; j increases downwards)[2].

Next, each component is addressed separately, and then coupled so that the full system can be solved. The equations are presented in the frequency domain, with each variable assuming a temporal variation of the type $\exp\left(\mathrm{i}\omega t\right)$, with ω being frequency, t time and i the imaginary unit. If damping is to be considered, then the bending stiffness of the rail and the elastic constants of the rail pads and under-sleeper pads shall be complex valued.

2.1. Ballast (and sub-grade)

Ballast is modelled as an assemblage of rigid masses interconnected by a regular network of horizontal, vertical and diagonal springs. Each mass has horizontal and vertical degrees of freedom, and their displacements are represented by $u_{x,i,j}$ and $u_{z,i,j}$, where the first index corresponds to the direction of the displacement (x is horizontal and z vertical), the second index to the column of the corresponding mass, and the third index to the row.

[2] Even though external moments at the rail and external forces applied directly at the ballast are unlikely in railway applications, the response to such excitations is needed for the derivation of absorbing boundaries. These absorbing boundaries are needed to expand the model here presented to the case in which there are variations in the stiffness of the support, which is the main motivation for the ongoing research (see Introduction). The derivation of the absorbing boundaries will be presented in a future publication, which will take as framework the equations derived in the present article.

The lattice type is as defined in the works by Suiker et al. [26,27], and a representation of an inner mass and its connections to the neighbouring masses is shown in Figure 2. For the horizontal and vertical springs, the stiffness constants for longitudinal and shear directions are $K^{\mathrm{n}}_{\mathrm{axi}}$ and $K^{\mathrm{s}}_{\mathrm{axi}}$, respectively, and for the diagonal springs the longitudinal and shear stiffness constants are $K^{\mathrm{n}}_{\mathrm{diag}} = \left(K^{\mathrm{n}}_{\mathrm{axi}} - K^{\mathrm{s}}_{\mathrm{axi}}\right)\big/2$ and $K^{\mathrm{s}}_{\mathrm{diag}} = 0$. These values must be complex valued if damping is to be considered.

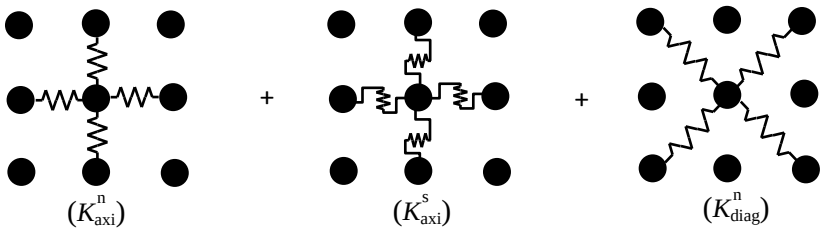

Figure 2. Detail of the interconnections of the lattice model for the ballast.

The vertical and horizontal distance between particles is the same (d) and is representative of the characteristic grain size of the particles forming the ballast. The mass of each particle (m_{b}) and the stiffness constants $K^{\mathrm{n}}_{\mathrm{axi}}$ and $K^{\mathrm{s}}_{\mathrm{axi}}$ must be chosen such that the lattice replicates the behaviour of ballast. If the ballast is assumed to behave as an elastic continuum, then guidelines for the definition of these values can be found in [27].

If the support of soil under the ballast is to be considered, then the lattice shall be layered, in which the first layer corresponds to ballast and the ones below correspond to each layer of soil and/or sub-ballast. The network of masses and springs remains regular and equally spaced (in this work we do not consider layered systems with different spacings, but in principle that is possible), but the properties to be assigned to each mass/spring depend on the properties of the specific layer that the part of the lattice refers to.

For the model depicted in Figure 1, besides the external forces $F_{\mathrm{v},e}$ and $F_{\mathrm{h},e}$ (not shown in the figure), the lattice is acted upon by forces $F^{\mathrm{usp}}_{l,n}$ that are transmitted from the sleeper l to the contact points $n = 0 \ldots N-1$, with the superscript usp standing for under-sleeper pad (see Figure 3). A positive force $F^{\mathrm{usp}}_{l,n}$ points upwards, which is the case when the under-sleeper spring is being stretched. For this combination of external and internal loads, the displacements $u_{x,i,j}$ and $u_{z,i,j}$ in the horizontal and vertical degrees of freedom of the generic mass at column i row j are calculated as

$$u_{x,i,j} = \sum_{l=-\infty}^{\infty} \sum_{n=0}^{N-1} u^{*}_{xz,i-l(N+M)-n,j,0} F^{\mathrm{usp}}_{l,n} + \sum_{e} u^{*}_{xx,i-i_e,j,j_e} F_{\mathrm{h},e} + \sum_{e} u^{*}_{xz,i-i_e,j,j_e} F_{\mathrm{v},e} \tag{1}$$

$$u_{z,i,j} = \sum_{l=-\infty}^{\infty} \sum_{n=0}^{N-1} u^{*}_{zz,i-l(N+M)-n,j,0} F^{\mathrm{usp}}_{l,n} + \sum_{e} u^{*}_{zx,i-i_e,j,j_e} F_{\mathrm{h},e} + \sum_{e} u^{*}_{zz,i-i_e,j,j_e} F_{\mathrm{v},e} \tag{2}$$

where $u^*_{\alpha\beta,p,q,r}$ is the displacement in the degree of freedom α of mass at column p and row q due to an unit (oscillating) load in direction β acting on the mass at column 0 and row r. The functions $u^*_{\alpha\beta,p,q,r}$ are the so called Green's functions of the lattice, and Suiker et al. [27] explain how they can be calculated. For the purpose of this work, and as will be explained later, it is of interest to know the Fourier Transform of these discrete functions, which can be found in Appendix A.

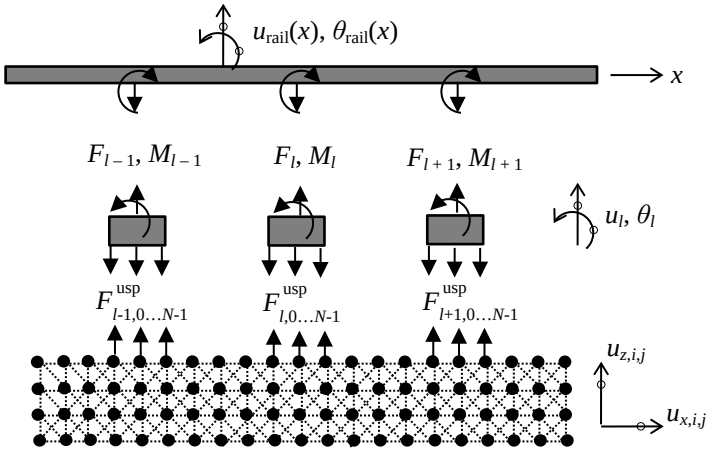

Figure 3. Under-sleeper pad and rail pad forces/moments. External forces/moments acting on the rail and lattice are not represented.

2.2. Sleepers

Sleepers are modelled as rigid masses with two degrees of freedom each, vertical translation and rotation (u_l and θ_l). The generic sleeper l, whose longitudinal position is $x_l = lL = l(N+M)d$, is acted upon by forces $F^{\text{usp}}_{l,n}$ exerted by the ballast via the under-sleeper pads, and by force F_l and moment M_l exerted by the rail via the rail pad (Figure 3). Positive values of $F^{\text{usp}}_{l,n}$ force the sleeper downwards, a positive force F_l forces the sleeper upwards (rail pad under tension) and a positive moment M_l forces the sleeper to rotate counter clockwise. Under these conditions, the vertical motion u_l and rotation motion θ_l of sleeper l is governed by the following two equations:

$$u_l = -\frac{1}{\omega^2 M_s}\left(-\sum_{n=0}^{N-1} F^{\text{usp}}_{l,n} + F_l\right) \tag{3}$$

$$\theta_l = -\frac{1}{\omega^2 J_s}\left(-\sum_{n=0}^{N-1} F^{\text{usp}}_{l,n} d\left[n-(N-1)/2\right] + M_l\right) \tag{4}$$

In the expression for θ_l, the factor $d\left[n-(N-1)/2\right]$ represents the distance of the contact point n to the middle of the sleeper.

2.3. Rail

The rail is modelled as a continuous Euler-Bernoulli beam. The beam is acted upon by the forces F_l (that force the rail downwards if positive) and moments M_l (that force the rail clockwise if positive) exerted by the rail pads (Figure 3), and by the external force $F_{\text{ext}}(x)$ and moment $M_{\text{ext}}(x)$ acting on it. Under these conditions, the vertical displacements $u_{\text{rail}}(x)$, rotations $\theta_{\text{rail}}(x)$, internal moment $M_{\text{rail}}(x)$ and internal shear $V_{\text{rail}}(x)$ of the rail are calculated by

$$\begin{aligned} u_{\text{rail}}(x) = &-\sum_{l=-\infty}^{+\infty} u^*_{\text{rail,F}}(x-x_l)F_l - \sum_{l=-\infty}^{+\infty} u^*_{\text{rail,M}}(x-x_l)M_l \\ &+\int_{-\infty}^{+\infty} u^*_{\text{rail,F}}(x-x_0)F_{\text{ext}}(x_0)\,\mathrm{d}x_0 + \int_{-\infty}^{+\infty} u^*_{\text{rail,M}}(x-x_0)M_{\text{ext}}(x_0)\,\mathrm{d}x_0 \end{aligned} \tag{5}$$

$$\begin{aligned} \theta_{\text{rail}}(x) = &-\sum_{l=-\infty}^{+\infty} \theta^*_{\text{rail,F}}(x-x_l)F_l - \sum_{l=-\infty}^{+\infty} \theta^*_{\text{rail,M}}(x-x_l)M_l \\ &+\int_{-\infty}^{+\infty} \theta^*_{\text{rail,F}}(x-x_0)F_{\text{ext}}(x_0)\,\mathrm{d}x_0 + \int_{-\infty}^{+\infty} \theta^*_{\text{rail,M}}(x-x_0)M_{\text{ext}}(x_0)\,\mathrm{d}x_0 \end{aligned} \tag{6}$$

$$\begin{aligned} M_{\text{rail}}(x) = &-\sum_{l=-\infty}^{+\infty} M^*_{\text{rail,F}}(x-x_l)F_l - \sum_{l=-\infty}^{+\infty} M^*_{\text{rail,M}}(x-x_l)M_l \\ &+\int_{-\infty}^{+\infty} M^*_{\text{rail,F}}(x-x_0)F_{\text{ext}}(x_0)\,\mathrm{d}x_0 + \int_{-\infty}^{+\infty} M^*_{\text{rail,M}}(x-x_0)M_{\text{ext}}(x_0)\,\mathrm{d}x_0 \end{aligned} \tag{7}$$

$$\begin{aligned} V_{\text{rail}}(x) = &-\sum_{l=-\infty}^{+\infty} V^*_{\text{rail,F}}(x-x_l)F_l - \sum_{l=-\infty}^{+\infty} V^*_{\text{rail,M}}(x-x_l)M_l \\ &+\int_{-\infty}^{+\infty} V^*_{\text{rail,F}}(x-x_0)F_{\text{ext}}(x_0)\,\mathrm{d}x_0 + \int_{-\infty}^{+\infty} V^*_{\text{rail,M}}(x-x_0)M_{\text{ext}}(x_0)\,\mathrm{d}x_0 \end{aligned} \tag{8}$$

where $u^*_{\text{rail,F}}(x)$, $\theta^*_{\text{rail,F}}(x)$, $M^*_{\text{rail,F}}(x)$ and $V^*_{\text{rail,F}}(x)$ are the Green's Functions of the rail (without any support) for displacements, rotations, internal moment and internal shear induced by an unit (oscillating) force at $x=0$, and $u^*_{\text{rail,M}}(x)$, $\theta^*_{\text{rail,M}}(x)$, $M^*_{\text{rail,M}}(x)$ and $V^*_{\text{rail,M}}(x)$ are the same but for an unit moment. Expressions for these functions can be found in many textbooks (e.g. [28]), and read

$$u^*_{\text{rail,F}}(x) = \frac{1}{4EI_{\text{rail}}\,\bar{k}^3}\left(-\mathrm{i}\,\mathrm{e}^{-\mathrm{i}\bar{k}|x|} - \mathrm{e}^{-\bar{k}|x|}\right) \tag{9}$$

$$\theta^*_{\text{rail,F}}(x) = \frac{\partial u^*_{\text{rail,F}}(x)}{\partial x} = \frac{\operatorname{sign}(x)}{4EI_{\text{rail}}\,\bar{k}^2}\left(-\mathrm{e}^{-\mathrm{i}\bar{k}|x|} + \mathrm{e}^{-\bar{k}|x|}\right) \tag{10}$$

$$M^*_{\text{rail,F}}(x) = EI_{\text{rail}}\frac{\partial^2 u^*_{\text{rail,F}}(x)}{\partial x^2} = \frac{1}{4\,\bar{k}}\left(\mathrm{i}\,\mathrm{e}^{-\mathrm{i}\bar{k}|x|} - \mathrm{e}^{-\bar{k}|x|}\right) \tag{11}$$

$$V^*_{\text{rail,F}}(x) = EI_{\text{rail}} \frac{\partial^3 u^*_{\text{rail,F}}(x)}{\partial x^3} = \frac{\text{sign}(x)}{4}\left(\text{e}^{-\text{i}\bar{k}|x|} + \text{e}^{-\bar{k}|x|}\right) \tag{12}$$

$$u^*_{\text{rail,M}}(x) = -\theta^*_{\text{rail,F}}(x) = \frac{\text{sign}(x)}{4EI_{\text{rail}}\,\bar{k}^2}\left(\text{e}^{-\text{i}\bar{k}|x|} - \text{e}^{-\bar{k}|x|}\right) \tag{13}$$

$$\theta^*_{\text{rail,M}}(x) = \frac{\partial u^*_{\text{rail,M}}(x)}{\partial x} = \frac{1}{4EI_{\text{rail}}\,\bar{k}}\left(-\text{ie}^{-\text{i}\bar{k}|x|} + \text{e}^{-\bar{k}|x|}\right) \tag{14}$$

$$M^*_{\text{rail,M}}(x) = EI_{\text{rail}} \frac{\partial^2 u^*_{\text{rail,M}}(x)}{\partial x^2} = \frac{\text{sign}(x)}{4}\left(-\text{e}^{-\text{i}\bar{k}|x|} - \text{e}^{-\bar{k}|x|}\right) \tag{15}$$

$$V^*_{\text{rail,M}}(x) = EI_{\text{rail}} \frac{\partial^3 u^*_{\text{rail,M}}(x)}{\partial x^3} = \frac{\bar{k}}{4}\left(\text{ie}^{-\text{i}\bar{k}|x|} + \text{e}^{-\bar{k}|x|}\right) \tag{16}$$

where $\bar{k} = \sqrt[4]{\omega^2 m_{\text{rail}} / EI_{\text{rail}}}$.

2.4. Compatibility of displacements between components

The motion of each component of the track has been written in terms of the interaction forces between them. In order to solve the coupled system, the displacement between components must be made compatible. In this way, the ballast grains under the sleepers must displace the same as the sleeper minus the deformation of the under-sleeper pad. For the contact point n' of sleeper l', this is achieved through the relationship

$$u_{z,l'(M+N)+n',0} = u_{l'} + d\left[n' - (N-1)/2\right]\theta_{l'} - F^{\text{usp}}_{l',n'}/K_{\text{usp}}, \quad n' = 0 \ldots N-1 \tag{17}$$

Likewise, the vertical translation and the rotation of the sleepers must match those of the rail minus the deformation of the rail pads. For the sleeper l', such relations are written by

$$u_{l'} = u_{\text{rail}}(x_{l'}) - F_{l'}/K_{\text{v}} \tag{18}$$

$$\theta_{l'} = \theta_{\text{rail}}(x_{l'}) - M_{l'}/K_{\theta} \tag{19}$$

Eqs. (1)-(6) can be substituted in (17)-(19) such that these are written in terms of the unknown interaction forces. The obtained set of equations is

$$\sum_{l=-\infty}^{\infty}\sum_{n=0}^{N-1} u^{*}_{zz,(l'-l)(N+M)+(n'-n),0,0} F^{\mathrm{usp}}_{l,n} + \sum_{e} u^{*}_{zx,l'(N+M)+n'-i_e,0,j_e} F_{\mathrm{h},e} + \sum_{e} u^{*}_{zz,l'(N+M)+n'-i_e,0,j_e} F_{\mathrm{v},e} =$$

$$-\frac{1}{\omega^2 M_{\mathrm{s}}}\left(-\sum_{n=0}^{N-1} F^{\mathrm{usp}}_{l',n} + F_{l'}\right)$$

$$-d\left[n'-(N-1)/2\right]\frac{1}{\omega^2 J_{\mathrm{s}}}\left(-\sum_{n=0}^{N-1} F^{\mathrm{usp}}_{l',n} d\left[n-(N-1)/2\right] + M_{l'}\right) \qquad (20)$$

$$-F^{\mathrm{usp}}_{l',n'}/K_{\mathrm{usp}}, \qquad n' = 0\ldots N-1$$

$$-\frac{1}{\omega^2 M_{\mathrm{s}}}\left(-\sum_{n=0}^{N-1} F^{\mathrm{usp}}_{l',n} + F_{l'}\right) = -\sum_{l=-\infty}^{+\infty} u^{*}_{\mathrm{rail,F}}\left(x_{l'}-x_l\right)F_l - \sum_{l=-\infty}^{+\infty} u^{*}_{\mathrm{rail,M}}\left(x_{l'}-x_l\right)M_l +$$

$$+\int_{-\infty}^{+\infty} u^{*}_{\mathrm{rail,F}}\left(x_{l'}-x_0\right)F_{\mathrm{ext}}\left(x_0\right)\mathrm{d}x_0 + \int_{-\infty}^{+\infty} u^{*}_{\mathrm{rail,M}}\left(x_{l'}-x_0\right)M_{\mathrm{ext}}\left(x_0\right)\mathrm{d}x_0 + \qquad (21)$$

$$-F_{l'}/K_{\mathrm{v}}$$

$$-\frac{1}{\omega^2 J_{\mathrm{s}}}\left(-\sum_{n=0}^{N-1} F^{\mathrm{usp}}_{l',n} d\left[n-(N-1)/2\right] + M_{l'}\right) =$$

$$-\sum_{l=-\infty}^{+\infty} \theta^{*}_{\mathrm{rail,F}}\left(x_{l'}-x_l\right)F_l - \sum_{l=-\infty}^{+\infty} \theta^{*}_{\mathrm{rail,M}}\left(x_{l'}-x_l\right)M_l +$$

$$+\int_{-\infty}^{+\infty} \theta^{*}_{\mathrm{rail,F}}\left(x_{l'}-x_0\right)F_{\mathrm{ext}}\left(x_0\right)\mathrm{d}x_0 + \int_{-\infty}^{+\infty} \theta^{*}_{\mathrm{rail,M}}\left(x_{l'}-x_0\right)M_{\mathrm{ext}}\left(x_0\right)\mathrm{d}x_0 + \qquad (22)$$

$$-M_{l'}/K_{\theta}$$

The N distinct variations of Eq. (20) accounting for all interaction particles ($n' = 0\ldots N-1$) can be written together with Eqs. (21)-(22) in the more convenient matrix form as

$$\sum_{l=-\infty}^{+\infty} \mathbf{U}_{l'-l}\mathbf{f}_l + \mathbf{E}\,\mathbf{f}_{l'} = \mathbf{u}_{l'} \qquad (23)$$

where the matrices and vectors have the following structures:

$$
\mathbf{U}_l = \begin{bmatrix} \mathbf{U}_l^{\text{lattice}} & \mathbf{O}_{N\times 2} \\ \mathbf{O}_{2\times N} & \mathbf{U}_l^{\text{rail}} \end{bmatrix}, \mathbf{E} = \begin{bmatrix} \mathbf{A} & \mathbf{C} \\ \mathbf{C}^{\mathrm{T}} & \mathbf{B} \end{bmatrix}, \mathbf{f}_l = \begin{bmatrix} \left\{ F_{l,n}^{\text{usp}} \right\} \downarrow^n \\ F_l \\ M_l \end{bmatrix}, \mathbf{u}_l = \begin{bmatrix} \mathbf{u}_l^{\text{lattice}} \\ \mathbf{u}_l^{\text{rail}} \end{bmatrix}
$$

$$
\mathbf{U}_l^{\text{lattice}} = \left\{ u^*_{zz,l(N+M)+(n'-n),0,0} \right\} \downarrow^{n'}, \mathbf{U}_l^{\text{rail}} = \begin{bmatrix} u^*_{\text{rail,F}}(x_l) & u^*_{\text{rail,M}}(x_l) \\ \theta^*_{\text{rail,F}}(x_l) & \theta^*_{\text{rail,M}}(x_l) \end{bmatrix}
$$

$$
\mathbf{A} = -\frac{1}{\omega^2 M_{\text{s}}} \overbrace{\{1\}}^{n} \downarrow^{n'} - \frac{d^2}{\omega^2 J_{\text{s}}} \left\{ \left[n' - (N-1)/2 \right] \overbrace{\left[n - (N-1)/2 \right]}^{n} \right\} \downarrow^{n'} + \text{diag}_{NxN} \left\{ \frac{1}{K_{\text{usp}}} \right\}
$$

$$
\mathbf{B} = \begin{bmatrix} -\frac{1}{\omega^2 M_{\text{s}}} + \frac{1}{K_{\text{v}}} & 0 \\ 0 & -\frac{1}{\omega^2 J_{\text{s}}} + \frac{1}{K_{\theta}} \end{bmatrix}, \quad \mathbf{C} = \left\{ \frac{1}{\omega^2 M_{\text{s}}} \quad \frac{\left[n' - (N-1)/2 \right] d}{\omega^2 J_{\text{s}}} \right\} \downarrow^{n'}
$$

$$
\mathbf{u}_l^{\text{lattice}} = -\left\{ \sum_e u^*_{zx,l'(N+M)+n'-i_e,0,j_e} F_{\text{h},e} + \sum_e u^*_{zz,l'(N+M)+n'-i_e,0,j_e} F_{\text{v},e} \right\} \downarrow^{n'}
$$

$$
\mathbf{u}_l^{\text{rail}} = \int_{-\infty}^{+\infty} \begin{bmatrix} u^*_{\text{rail,F}}(x_l - x_0) & u^*_{\text{rail,M}}(x_l - x_0) \\ \theta^*_{\text{rail,F}}(x_l - x_0) & \theta^*_{\text{rail,M}}(x_l - x_0) \end{bmatrix} \begin{bmatrix} F_{\text{ext}}(x_0) \\ M_{\text{ext}}(x_0) \end{bmatrix} \mathrm{d}x_0
$$

$$
n', n = 0 \ldots N-1 \tag{24}
$$

2.5. Transformation to the wavenumber domain

System of equations (23) gives an expression relating the interaction forces at each sleeper with the external excitation. The equation may be solved as it is for the interaction forces by truncating the domain to a certain number of sleepers. That, however, results in an augmented system of equations that can become very large, depending on how many sleepers are considered. Alternatively, system (23) can be transformed to the wavenumber domain by means of the Fourier transform of discrete functions [29] (also called Floquet transform, as in [25]). For the problem at hand, the application of the Fourier transform leads to

$$
\left[\tilde{\mathbf{U}}(k) + \mathbf{E} \right] \tilde{\mathbf{f}}(k) = \tilde{\mathbf{u}}(k) \tag{25}
$$

where

$$
\tilde{\mathbf{U}}(k) = \sum_{l=-\infty}^{+\infty} \mathbf{U}_l \mathrm{e}^{\mathrm{i}k\,x_l} \tag{26}
$$

$$
\tilde{\mathbf{u}}(k) = \begin{bmatrix} \tilde{\mathbf{u}}^{\text{lattice}}(k) \\ \tilde{\mathbf{u}}^{\text{rail}}(k) \end{bmatrix} = \sum_{l=-\infty}^{+\infty} \begin{bmatrix} \mathbf{u}_l^{\text{lattice}} \\ \mathbf{u}_l^{\text{rail}} \end{bmatrix} \mathrm{e}^{\mathrm{i}k\,x_l} \tag{27}
$$

$$
\tilde{\mathbf{f}}(k) = \begin{bmatrix} \left\{ \tilde{F}_n^{\text{usp}}(k) \right\} \downarrow^n \\ \tilde{F}(k) \\ \tilde{M}(k) \end{bmatrix} = \sum_{l=-\infty}^{+\infty} \begin{bmatrix} \left\{ F_{l,n}^{\text{usp}} \right\} \downarrow^n \\ F_l \\ M_l \end{bmatrix} \mathrm{e}^{\mathrm{i}k\,x_l} \tag{28}
$$

2.5.1. Evaluation of $\tilde{\mathbf{U}}^{\text{rail}}(k)$ and $\tilde{\mathbf{U}}^{\text{lattice}}(k)$

Due to the structure of $\mathbf{U}_l$, the infinite sum needed to calculate matrix $\tilde{\mathbf{U}}(k)$ can be evaluated analytically. Starting with the submatrix $\mathbf{U}_l^{\text{rail}}$, its Fourier transform is

$$\tilde{\mathbf{U}}^{\text{rail}}(k)=\sum_{l=-\infty}^{+\infty}\mathbf{U}_l^{\text{rail}}\mathrm{e}^{\mathrm{i}k\,x_l}=\frac{1}{4EI_{\text{rail}}}\begin{bmatrix}\frac{-\mathrm{i}a(\mathrm{i}\bar{k},k)-a(\bar{k},k)}{\bar{k}^3} & \frac{b(\mathrm{i}\bar{k},k)-b(\bar{k},k)}{\bar{k}^2}\\ \frac{-b(\mathrm{i}\bar{k},k)+b(\bar{k},k)}{\bar{k}^2} & \frac{-\mathrm{i}a(\mathrm{i}\bar{k},k)+a(\bar{k},k)}{\bar{k}}\end{bmatrix} \tag{29}$$

where $\bar{k}$ is as defined below Eq. (16) and where

$$a(k_1,k_2)=\sum_{l=-\infty}^{+\infty}\mathrm{e}^{-k_1|x_l|}\mathrm{e}^{\mathrm{i}k_2x_l}=\frac{\mathrm{e}^{(\mathrm{i}k_2-k_1)L}-\mathrm{e}^{(\mathrm{i}k_2+k_1)L}}{\left(\mathrm{e}^{k_1L}-\mathrm{e}^{\mathrm{i}k_2L}\right)\left(\mathrm{e}^{-k_1L}-\mathrm{e}^{\mathrm{i}k_2L}\right)} \tag{30}$$

$$b(k_1,k_2)=\sum_{l=-\infty}^{+\infty}\operatorname{sign}(x_l)\mathrm{e}^{-k_1|x_l|}\mathrm{e}^{\mathrm{i}k_2x_l}=\frac{\mathrm{e}^{(k_1+\mathrm{i}k_2)L}-\mathrm{e}^{(k_1-\mathrm{i}k_2)L}}{\left(\mathrm{e}^{k_1L}-\mathrm{e}^{\mathrm{i}k_2L}\right)\left(\mathrm{e}^{k_1L}-\mathrm{e}^{-\mathrm{i}k_2L}\right)}=-a(\mathrm{i}k_2,-\mathrm{i}k_1) \tag{31}$$

The sums in Eqs. (30)-(31) represent convergent infinite geometric series, and were evaluated with the help of Wolfram|Alpha [30].

Regarding the submatrix $\mathbf{U}_l^{\text{lattice}}$, formed by the lattice Green's functions $u^*_{zz,l(N+M)+(n'-n),0,0}$, its Fourier transform $\tilde{\mathbf{U}}^{\text{lattice}}$ is composed by the components $\tilde{u}^*_{n'n}(k)$ (the first index refers to the row, while the second index refers to the column of $\tilde{\mathbf{U}}^{\text{lattice}}$) calculated with

$$\begin{aligned}\tilde{u}^*_{n'n}(k)&=\sum_{l=-\infty}^{+\infty}u^*_{zz,l(N+M)+(n'-n),0,0}\,\mathrm{e}^{\mathrm{i}\,k\,x_l}=\\&\frac{1}{M+N}\sum_{m=0}^{M+N-1}\bar{u}^*_{zz,0,0}(\kappa_m)\mathrm{e}^{-\mathrm{i}\kappa_m d(n'-n)}\end{aligned} \tag{32}$$

where $\kappa_m=k-\frac{2\pi m}{L}$ is the lattice wavenumber and $\bar{u}^*_{zz,p,q}(\kappa_m)$ is the vertical response of the lattice at its elevation p due to a vertical load at elevation q in the wavenumber domain. Appendix A explains how to calculate these wavenumber domain Green's functions. The second statement in (32) comes after the down sampling (decimation) and shift properties of the Fourier transform of discrete signals [29], and even though κ_m and k have the same dimensions, they are associated with signals with different sampling periods, the former with periodicity d, and the latter with periodicity $L=(M+N)d$.

2.5.2. Evaluation of $\tilde{\mathbf{u}}^{\text{lattice}}(k)$

The missing term for the calculation of the unknown forces $\tilde{\mathbf{f}}(k)$ in Eq. (25) is the displacement field $\tilde{\mathbf{u}}(k)$ induced by the external forces. The expression for its calculation is given in Eq. (27). There are two components for the displacements $\tilde{\mathbf{u}}(k)$: the displacement field induced by

the external forces acting on the lattice, $\tilde{\mathbf{u}}^{\text{lattice}}(k)$, and those induced by external forces/moments at the rail, $\tilde{\mathbf{u}}^{\text{rail}}(k)$. The component n' of $\tilde{\mathbf{u}}^{\text{lattice}}(k)$, $\tilde{u}_{n'}^{\text{lattice}}(k)$, is calculated with

$$\tilde{u}_{n'}^{\text{lattice}}(k) = -\sum_{e} \begin{bmatrix} F_{\text{h},e} \\ F_{\text{v},e} \end{bmatrix}^{\text{T}} \sum_{l=-\infty}^{+\infty} \text{e}^{\text{i}\,k\,x_l} \begin{bmatrix} u^*_{zx,l(N+M)+n'-i_e,0,j_e} \\ u^*_{zz,l(N+M)+n'-i_e,0,j_e} \end{bmatrix} \tag{33}$$

and after taking into account the down sampling and shift properties also used in Eq. (32), $\tilde{u}_{n'}^{\text{lattice}}(k)$ simplifies to

$$\tilde{u}_{n'}^{\text{lattice}}(k) = -\frac{1}{M+N} \sum_{e} \begin{bmatrix} F_{\text{h},e} \\ F_{\text{v},e} \end{bmatrix}^{\text{T}} \sum_{m=0}^{M+N-1} \begin{bmatrix} \overline{u}^*_{zx,0,j_e}(\kappa_m) \\ \overline{u}^*_{zz,0,j_e}(\kappa_m) \end{bmatrix} \text{e}^{-\text{i}\kappa_m d(n'-i_e)} \tag{34}$$

Again, $\kappa_m = k - \frac{2\pi m}{L}$ and $\overline{u}^*_{zx,p,q}(\kappa_m)$ and $\overline{u}^*_{zz,p,q}(\kappa_m)$ are the wavenumber domain Green's functions of the lattice.

2.5.3. Evaluation of $\tilde{\mathbf{u}}^{\text{rail}}(k)$ – non-moving load

For loads $F_{\text{ext}}(x)$ and moments $M_{\text{ext}}(x)$ with arbitrary distribution, vector $\mathbf{u}_l^{\text{rail}}$ resulting from the integral in Eq. (24) cannot be evaluated analytically. However, for the particular cases of non-moving point disturbances or harmonic disturbances moving with constant speed, the integrals can be evaluated analytically in closed-form expressions. For the non-moving case, in which $F_{\text{ext}}(x) = F_p \delta(x - x_p)$ and $M_{\text{ext}}(x) = M_p \delta(x - x_p)$, where $\delta(x)$ is the Dirac delta function, F_p and M_p are the force and moment amplitudes, and x_p is the coordinate of the loaded point, the component $\mathbf{u}_l^{\text{rail}}$ simplifies to

$$\mathbf{u}_l^{\text{rail}} = \begin{bmatrix} u^*_{\text{rail,F}}(x_l - x_p) & u^*_{\text{rail,M}}(x_l - x_p) \\ \theta^*_{\text{rail,F}}(x_l - x_p) & \theta^*_{\text{rail,M}}(x_l - x_p) \end{bmatrix} \begin{bmatrix} F_p \\ M_p \end{bmatrix} \tag{35}$$

and its Fourier transform $\tilde{\mathbf{u}}^{\text{rail}}(k)$, according to Eq. (27), is

$$\tilde{\mathbf{u}}^{\text{rail}}(k) = \frac{1}{4EI_{\text{rail}}} \begin{bmatrix} \frac{-\text{i}\,c(\text{i}\bar{k},k,x_p) - c(\bar{k},k,x_p)}{\bar{k}^3} & \frac{d(\text{i}\bar{k},k,x_p) - d(\bar{k},k,x_p)}{\bar{k}^2} \\ \frac{-d(\text{i}\bar{k},k,x_p) + d(\bar{k},k,x_p)}{\bar{k}^2} & \frac{-\text{ic}(\text{i}\bar{k},k,x_p) + c(\bar{k},k,x_p)}{\bar{k}} \end{bmatrix} \begin{bmatrix} F_p \\ M_p \end{bmatrix} \tag{36}$$

where

$$c(k_1,k_2,x) = \sum_{l=-\infty}^{+\infty} \text{e}^{-k_1|x_l - x|} \text{e}^{\text{i}\,k_2\,x_l} = \text{e}^{\text{i}k_2 L(X+1)} \left(\frac{\text{e}^{k_1(x-XL)}}{\text{e}^{k_1 L} - \text{e}^{\text{i}k_2 L}} - \frac{\text{e}^{-k_1(x-XL)}}{\text{e}^{-k_1 L} - \text{e}^{\text{i}k_2 L}} \right) \tag{37}$$

$$d(k_1,k_2,x) = \sum_{l=-\infty}^{+\infty} \text{sign}(x_l - x) \text{e}^{-k_1|x_l - x|} \text{e}^{\text{i}\,k_2 x_l} = \text{e}^{\text{i}k_2 L(X+1)} \left(\frac{\text{e}^{k_1(x-XL)}}{\text{e}^{k_1 L} - \text{e}^{\text{i}k_2 L}} + \frac{\text{e}^{-k_1(x-XL)}}{\text{e}^{-k_1 L} - \text{e}^{\text{i}k_2 L}} \right) \tag{38}$$

In Eqs. (37)-(38), X is the rounding off of $\frac{x}{L}$ to its nearest integer towards minus infinity.

2.5.4. Evaluation of $\tilde{\mathbf{u}}^{\text{rail}}(k)$ –moving load with constant speed

For point disturbances moving with speed V, oscillating with frequency ω_0, and with amplitudes F_0 and M_0, i.e., $F(x,t)=F_0\exp(\mathrm{i}\omega_0 t)\delta(x-Vt)$ and $M(x,t)=M_0\exp(\mathrm{i}\omega_0 t)\delta(x-Vt)$, the corresponding frequency domain forces are

$$\begin{aligned} F_{\text{ext}}(x) &= F_0\int_{-\infty}^{+\infty}\delta(x-Vt)\mathrm{e}^{\mathrm{i}(\omega_0-\omega)t}\mathrm{d}t=\frac{F_0}{V}\mathrm{e}^{\mathrm{i}(\omega_0-\omega)\frac{x}{V}} \\ M_{\text{ext}}(x) &= M_0\int_{-\infty}^{+\infty}\delta(x-Vt)\mathrm{e}^{\mathrm{i}(\omega_0-\omega)t}\mathrm{d}t=\frac{M_0}{V}\mathrm{e}^{\mathrm{i}(\omega_0-\omega)\frac{x}{V}} \end{aligned} \tag{39}$$

For these load types, the integral in (24) results in (see Appendix B)

$$\begin{aligned} \mathbf{u}_l^{\text{rail}} &= \int_{-\infty}^{+\infty}\begin{bmatrix} u^*_{\text{rail,F}}(x_l-x_0) & u^*_{\text{rail,M}}(x_l-x_0) \\ \theta^*_{\text{rail,F}}(x_l-x_0) & \theta^*_{\text{rail,M}}(x_l-x_0)\end{bmatrix}\begin{bmatrix} F_{\text{ext}}(x_0) \\ M_{\text{ext}}(x_0)\end{bmatrix}\mathrm{d}x_0 \\ &= \frac{\mathrm{e}^{-\mathrm{i}\frac{\omega-\omega_0}{V}x_l}}{V\left[\left(\frac{\omega-\omega_0}{V}\right)^4 EI_{\text{rail}}-\omega^2 m_{\text{rail}}\right]}\begin{bmatrix} 1 & \mathrm{i}\frac{\omega-\omega_0}{V} \\ -\mathrm{i}\frac{\omega-\omega_0}{V} & \left(\frac{\omega-\omega_0}{V}\right)^2\end{bmatrix}\begin{bmatrix} F_0 \\ M_0\end{bmatrix} \end{aligned} \tag{40}$$

and its Fourier transform, according to (27), is

$$\tilde{\mathbf{u}}^{\text{rail}}(k)=\frac{1}{V\left[\left(\frac{\omega-\omega_0}{V}\right)^4 EI_{\text{rail}}-\omega^2 m_{\text{rail}}\right]}\begin{bmatrix} 1 & \mathrm{i}\frac{\omega-\omega_0}{V} \\ -\mathrm{i}\frac{\omega-\omega_0}{V} & \left(\frac{\omega-\omega_0}{V}\right)^2\end{bmatrix}\begin{bmatrix} F_0 \\ M_0\end{bmatrix}\frac{2\pi}{L}\sum_{h=-\infty}^{+\infty}\delta\left(\frac{\omega-\omega_0}{V}-k-\frac{2\pi h}{L}\right) \tag{41}$$

2.6. Transformation back to the space domain

2.6.1. Response of the sleepers

From Eq. (25), $\tilde{\mathbf{f}}(k)$ can be readily available, and from there the vector force $\mathbf{f}_l$ at reference cell l can be calculated via

$$\mathbf{f}_l=\frac{L}{2\pi}\int_{k_{\text{ref}}-\frac{\pi}{L}}^{k_{\text{ref}}+\frac{\pi}{L}}\tilde{\mathbf{f}}(k)\mathrm{e}^{-\mathrm{i}k x_l}\mathrm{d}k \tag{42}$$

where k_{ref} can be any real wavenumber. Eq. (42) implies a wavenumber integration over a single Brillouin zone [31]: it is the inverse of the forward transform specified in Eq. (28).

For a generic external excitation composed of forces applied at the lattice and at the rail, the integral in Eq. (42) has to be evaluated numerically. For the specific case in which only moving disturbances at the rail are applied, the integral can be evaluated analytically (due to the presence of the Dirac functions). That case is addressed in Section 4.

After evaluating Eq. (42), the response of the sleepers can be readily available by substituting the obtained forces $\mathbf{f}_l$ in the equations of motion of the sleeper, Eqs. (3) and (4). Likewise, the translations and rotations of the rail at the contact points with the sleepers can be obtained by satisfying the compatibility conditions specified in Eqs. (18) and (19), for which sleeper motions and interaction forces (rail pad forces) are already known.

2.6.2. Response of the rail

If the response of the rail at positions other than the sleeper positions is of interest, then its response must be calculated from Eqs. (5)-(8). There are two components contributing to the response: the one induced by the external forces (moving or non-moving) and the one induced by the rail pad forces (F_l and M_l). For the case of stationary external disturbances, the contribution of the first component is given by

$$\mathbf{u}^{\text{rail}}_{F_p\oplus M_p}\left(x\right)=\begin{bmatrix} u^{\text{rail}}_{F_p\oplus M_p}\left(x\right)\\ \theta^{\text{rail}}_{F_p\oplus M_p}\left(x\right)\end{bmatrix}=\begin{bmatrix} u^{*}_{\text{rail,F}}\left(x-x_p\right) & u^{*}_{\text{rail,M}}\left(x-x_p\right)\\ \theta^{*}_{\text{rail,F}}\left(x-x_p\right) & \theta^{*}_{\text{rail,M}}\left(x-x_p\right)\end{bmatrix}\begin{bmatrix} F_p\\ M_p\end{bmatrix} \tag{43}$$

$$\mathbf{s}^{\text{rail}}_{F_p\oplus M_p}\left(x\right)=\begin{bmatrix} M^{\text{rail}}_{F_p\oplus M_p}\left(x\right)\\ V^{\text{rail}}_{F_p\oplus M_p}\left(x\right)\end{bmatrix}=\begin{bmatrix} M^{*}_{\text{rail,F}}\left(x-x_p\right) & M^{*}_{\text{rail,M}}\left(x-x_p\right)\\ V^{*}_{\text{rail,F}}\left(x-x_p\right) & V^{*}_{\text{rail,M}}\left(x-x_p\right)\end{bmatrix}\begin{bmatrix} F_p\\ M_p\end{bmatrix} \tag{44}$$

and for the case of moving disturbances, the contribution is given by

$$\mathbf{u}^{\text{rail}}_{F_0\oplus M_0}\left(x\right)=\begin{bmatrix} u^{\text{rail}}_{F_0\oplus M_0}\left(x\right)\\ \theta^{\text{rail}}_{F_0\oplus M_0}\left(x\right)\end{bmatrix}=\frac{\mathrm{e}^{-\mathrm{i}\frac{\omega-\omega_0}{V}x}}{V\left[\left(\frac{\omega-\omega_0}{V}\right)^4 EI_{\text{rail}}-\omega^2 m_{\text{rail}}\right]}\begin{bmatrix} 1 & \mathrm{i}\frac{\omega-\omega_0}{V}\\ -\mathrm{i}\frac{\omega-\omega_0}{V} & \left(\frac{\omega-\omega_0}{V}\right)^2\end{bmatrix}\begin{bmatrix} F_0\\ M_0\end{bmatrix} \tag{45}$$

$$\mathbf{s}^{\text{rail}}_{F_0\oplus M_0}\left(x\right)=\begin{bmatrix} M^{\text{rail}}_{F_0\oplus M_0}\left(x\right)\\ V^{\text{rail}}_{F_0\oplus M_0}\left(x\right)\end{bmatrix}=\frac{\mathrm{e}^{-\mathrm{i}\frac{\omega-\omega_0}{V}x}}{V\left[\left(\frac{\omega-\omega_0}{V}\right)^4 EI_{\text{rail}}-\omega^2 m_{\text{rail}}\right]}\begin{bmatrix} -\left(\frac{\omega-\omega_0}{V}\right)^2 & -\mathrm{i}\left(\frac{\omega-\omega_0}{V}\right)^3\\ \mathrm{i}\left(\frac{\omega-\omega_0}{V}\right)^3 & -\left(\frac{\omega-\omega_0}{V}\right)^4\end{bmatrix}\begin{bmatrix} F_0\\ M_0\end{bmatrix} \tag{46}$$

The symbol $\oplus$ is used to indicate that the response is the combined action of the forces and moments.

The evaluation of the contribution of the second component ($\mathbf{u}^{\text{rail}}_{\text{rp}}$, rp standing for rail pad forces) requires calculating an infinite sum, i.e.,

$$\mathbf{u}^{\text{rail}}_{\text{rp}}\left(x\right)=\begin{bmatrix} u^{\text{rail}}_{\text{rp}}\left(x\right)\\ \theta^{\text{rail}}_{\text{rp}}\left(x\right)\end{bmatrix}=-\sum_{l=-\infty}^{+\infty}\begin{bmatrix} u^{*}_{\text{rail,F}}\left(x-x_l\right) & u^{*}_{\text{rail,M}}\left(x-x_l\right)\\ \theta^{*}_{\text{rail,F}}\left(x-x_l\right) & \theta^{*}_{\text{rail,M}}\left(x-x_l\right)\end{bmatrix}\begin{bmatrix} F_l\\ M_l\end{bmatrix} \tag{47}$$

$$\mathbf{s}^{\text{rail}}_{\text{sp}}\left(x\right)=\begin{bmatrix} M^{\text{rail}}_{\text{rp}}\left(x\right)\\ V^{\text{rail}}_{\text{rp}}\left(x\right)\end{bmatrix}=-\sum_{l=-\infty}^{+\infty}\begin{bmatrix} M^{*}_{\text{rail,F}}\left(x-x_l\right) & M^{*}_{\text{rail,M}}\left(x-x_l\right)\\ V^{*}_{\text{rail,F}}\left(x-x_l\right) & V^{*}_{\text{rail,M}}\left(x-x_l\right)\end{bmatrix}\begin{bmatrix} F_l\\ M_l\end{bmatrix} \tag{48}$$

The rail pad forces F_l and M_l are obtained by the integral (42), and if that integral is inserted in Eqs. (47)-(48), then the infinite summation can be replaced by a finite integral:

$$\begin{aligned}\mathbf{u}_{\mathrm{rp}}^{\mathrm{rail}}\left(x\right)&=-\frac{L}{2\pi}\int_{k_{\mathrm{ref}}-\frac{\pi}{L}}^{k_{\mathrm{ref}}+\frac{\pi}{L}}\sum_{l=-\infty}^{+\infty}\begin{bmatrix}u_{\mathrm{rail,F}}^{*}\left(x-x_l\right) & u_{\mathrm{rail,M}}^{*}\left(x-x_l\right)\\ \theta_{\mathrm{rail,F}}^{*}\left(x-x_l\right) & \theta_{\mathrm{rail,M}}^{*}\left(x-x_l\right)\end{bmatrix}\mathrm{e}^{-\mathrm{i}\,k\,x_l}\begin{bmatrix}\tilde{F}\left(k\right)\\ \tilde{M}\left(k\right)\end{bmatrix}\mathrm{d}k\\&=-\frac{L}{8\pi EI_{\mathrm{rail}}}\int_{k_{\mathrm{ref}}-\frac{\pi}{L}}^{k_{\mathrm{ref}}+\frac{\pi}{L}}\begin{bmatrix}\frac{-\mathrm{i}\,c\left(\mathrm{i}\bar{k},k,-x\right)-c\left(\bar{k},k,-x\right)}{\bar{k}^3} & \frac{d\left(\mathrm{i}\bar{k},k,-x\right)-d\left(\bar{k},k,-x\right)}{\bar{k}^2}\\ \frac{-d\left(\mathrm{i}\bar{k},k,-x\right)+d\left(\bar{k},k,-x\right)}{\bar{k}^2} & \frac{-\mathrm{i}c\left(\mathrm{i}\bar{k},k,-x\right)+c\left(\bar{k},k,-x\right)}{\bar{k}}\end{bmatrix}\begin{bmatrix}\tilde{F}\left(k\right)\\ \tilde{M}\left(k\right)\end{bmatrix}\mathrm{d}k\end{aligned}\tag{49}$$

$$\begin{aligned}\mathbf{s}_{\mathrm{rp}}^{\mathrm{rail}}\left(x\right)&=-\frac{L}{2\pi}\int_{k_{\mathrm{ref}}-\frac{\pi}{L}}^{k_{\mathrm{ref}}+\frac{\pi}{L}}\sum_{l=-\infty}^{+\infty}\begin{bmatrix}M_{\mathrm{rail,F}}^{*}\left(x-x_l\right) & M_{\mathrm{rail,M}}^{*}\left(x-x_l\right)\\ V_{\mathrm{rail,F}}^{*}\left(x-x_l\right) & V_{\mathrm{rail,M}}^{*}\left(x-x_l\right)\end{bmatrix}\mathrm{e}^{-\mathrm{i}\,k\,x_l}\begin{bmatrix}\tilde{F}\left(k\right)\\ \tilde{M}\left(k\right)\end{bmatrix}\mathrm{d}k\\&=-\frac{L\,\bar{k}^2}{8\pi}\int_{k_{\mathrm{ref}}-\frac{\pi}{L}}^{k_{\mathrm{ref}}+\frac{\pi}{L}}\begin{bmatrix}\frac{\mathrm{i}\,c\left(\mathrm{i}\bar{k},k,-x\right)-c\left(\bar{k},k,-x\right)}{\bar{k}^3} & \frac{-d\left(\mathrm{i}\bar{k},k,-x\right)-d\left(\bar{k},k,-x\right)}{\bar{k}^2}\\ \frac{d\left(\mathrm{i}\bar{k},k,-x\right)+d\left(\bar{k},k,-x\right)}{\bar{k}^2} & \frac{\mathrm{i}\,c\left(\mathrm{i}\bar{k},k,-x\right)+c\left(\bar{k},k,-x\right)}{\bar{k}}\end{bmatrix}\begin{bmatrix}\tilde{F}\left(k\right)\\ \tilde{M}\left(k\right)\end{bmatrix}\mathrm{d}k\end{aligned}\tag{50}$$

2.6.3. Response of the lattice

As in the case of the rail response, there are two sources contributing to the total response of the lattice: the externally applied forces ($F_{\mathrm{h},e}$, $F_{\mathrm{v},e}$) and the interaction forces between sleepers and lattice (under-sleeper pad forces, $F_{l,n}^{\mathrm{usp}}$) – see Eqs. (1) and (2). The contribution $u_{\alpha,i,j}^{\mathrm{ext}}$ of the external forces to the displacements of the generic mass i,j in direction α is calculated with

$$\begin{aligned}u_{\alpha,i,j}^{\mathrm{ext}}&=\sum_e u_{\alpha x,i-i_e,j,j_e}^{*}F_{\mathrm{h},e}+\sum_e u_{\alpha z,i-i_e,j,j_e}^{*}F_{\mathrm{v},e}\\&=\frac{d}{2\pi}\sum_e\int_{\kappa_{ref}-\frac{\pi}{d}}^{\kappa_{ref}+\frac{\pi}{d}}\begin{bmatrix}\bar{u}_{\alpha x,j,j_e}^{*}\left(\kappa\right) & \bar{u}_{\alpha z,j,j_e}^{*}\left(\kappa\right)\end{bmatrix}\begin{bmatrix}F_{\mathrm{h},e}\\ F_{\mathrm{v},e}\end{bmatrix}\mathrm{e}^{-\mathrm{i}\kappa\left(i-i_e\right)d}\mathrm{d}\kappa\end{aligned}\tag{51}$$

where $\bar{u}_{\alpha\beta,p,q}^{*}\left(\kappa\right)$ ($\alpha,\beta=x,z$) are the lattice Green's functions in the wavenumber domain and as explained in Appendix A. Note that the integration in Eq. (51) is over one Brillouin region defined based on the lattice periodicity (d), which is different from that in Eq. (42).

Regarding the contribution $u_{\alpha,i,j}^{\mathrm{usp}}$ resulting from the under-sleeper pads forces to the motion of the mass i,j in direction α , in principle it can be obtained by evaluating the infinite summation in (1)-(2). That, however, requires the truncation of the number of sleepers to be considered, not to mention the great computation effort it entails. A more elegant alternative is to multiply the convoluted signals in the wavenumber domain and then transform the solution back to space. In this way, $u_{\alpha,i,j}^{\mathrm{usp}}$ can be calculated with

$$u_{\alpha,i,j}^{\mathrm{usp}}=\frac{d}{2\pi}\int_{\kappa_{\mathrm{ref}}-\frac{\pi}{d}}^{\kappa_{\mathrm{ref}}+\frac{\pi}{d}}\bar{u}_{\alpha z,j,0}^{*}\left(\kappa\right)\tilde{F}^{\mathrm{usp}}\left(\kappa\right)\mathrm{e}^{-\mathrm{i}\,\kappa\,i\,d}\mathrm{d}\kappa\tag{52}$$

where $\tilde{F}^{\text{usp}}(\kappa)$ is the Fourier transform (based on the lattice spacing) of the set of forces transmitted by all sleepers to the lattice, calculated as

$$\tilde{F}^{\text{usp}}(\kappa) = \sum_{l=-\infty}^{+\infty} \sum_{n=0}^{N-1} F_{l,n}^{\text{usp}} \mathrm{e}^{\mathrm{i}\kappa(x_l + n\,d)} \tag{53}$$

Though the wavenumbers κ in $\tilde{F}^{\text{usp}}(\kappa)$ and $\tilde{F}_n^{\text{usp}}(k)$ – see Eq. (28) – have the same dimensions, these variables result from transforming signals with different sampling periodicities, the former with periodicity d and the latter with periodicity $L = (N+M)d$. Thus, $\tilde{F}^{\text{usp}}(\kappa)$ and $\tilde{F}_n^{\text{usp}}(k)$ are related through the time expansion and shift properties of the Fourier transform of discrete signals [29]. The relation between the two is

$$\tilde{F}^{\text{usp}}(\kappa) = \sum_{n=0}^{N-1} \tilde{F}_n^{\text{usp}}(k=\kappa) \mathrm{e}^{\mathrm{i}\,\kappa\,n\,d} \tag{54}$$

3. Dispersion of the railway track

Before verifying the equations obtained in Section 2 by means of an example involving a moving load, one first wants to point out that matrix $\mathbf{D} = \tilde{\mathbf{U}}(k) + \mathbf{E}$ in Eq. (25) may become singular for specific values of k and ω. These pairs of values represent frequencies and wavenumbers at which free waves can exist in the track, propagating or standing. In fact, these values of k (for a given frequency ω) are used in Floquet's theory to define the propagation factors from one span to the others as [20]

$$f(x + nL) = f(x) \mathrm{e}^{\mathrm{i}nkL} \tag{55}$$

where $f(x)$ represents the longitudinal dependence of any variable associated with the system (rail displacement/rotation or internal force, support reaction, etc.). Thus, the application of Floquet's theory requires finding these eigenvalues (that can be complex) and associated modal shapes, which for the problem at hand is not a trivial task since it involves solving non-algebraic eigenvalue problems (observe the exponential functions involving k in the definition of matrices $\tilde{\mathbf{U}}^{\text{rail}}$ and $\tilde{\mathbf{U}}^{\text{lattice}}$). For the solution method described in Section 2, these eigenpairs are not required, still they provide useful information about the dynamic behaviour of the system. For example, real valued pairs (ω, k) represent guided waves that propagate along the track with phase speed ω/k. Also, for lightly damped systems, for each frequency ω, the eigenvalues k indicate where sharp peaks may be encountered when evaluating the inverse Fourier integrals. The lines connecting the real valued pairs (ω, k) are termed dispersion lines.

In what follows, the dispersion lines are calculated for a track whose properties are taken from the work by Nordborg [20]: $EI_{\text{rail}} = 1.234 \times 10^6$ N m^2; $m_{\text{rail}} = 52$ kg/m; $M_{\text{s}} = 250$ kg; $K_{\text{v}} = 500 \times 10^6$ N/m;. $K_{\text{ballast}} = 42.5 \times 10^6$ N/m (lumped ballast). The mass of the sleeper and stiffness of the ballast correspond to one half of the track only, since only one rail is modelled. For the calculation of the dispersion lines, no damping is considered. In the reference work, the sleeper

only responds in the vertical direction; this condition is achieved in this work by setting the stiffness K_θ to zero and the rotational inertia J_s to infinity, and by removing from matrix $\mathbf{D}$ the last row (associated with the compatibility of rotations between sleepers and rail) and column (associated with moments M_l).

Two situations are considered: one in which the ballast is modelled together with the under-sleeper pads as a single spring (same situation as in the reference work; lumped ballast), and one in which ballast is modelled as a lattice whose depth is $H = 0.6\,\mathrm{m}$ and with particle diameter $d = 0.05\,\mathrm{m}$. The sleeper spacing is set at $L = 0.6\,\mathrm{m}$, and so there are $N = 7$ contact points between sleepers and ballast and $M = 5$ free ballast particles between sleepers. All masses of the lower surface of the lattice are impeded from moving in any direction, thus simulating that the ballast rests on a stiff foundation.

3.1. Ballast as localized springs (lumped)

For this scenario, the lattice is assumed rigid, and therefore matrices $\mathbf{U}_l^{\text{lattice}}$ and their transform $\tilde{\mathbf{U}}^{\text{lattice}}$ are composed of zeros. Also, the values of the under-sleeper pads K_{usp} must be such that the added stiffness of all N contact points matches the stiffness K_{ballast} (which results in $K_{\text{usp}} = 6.07\times10^6\ \mathrm{N/m}$). For these values, and for wavenumbers k ranging from 0 to $\pi/L \approx 5.3\,\mathrm{rad/m}$ (one half of the Brillouin region; the lines are mirrored beyond this value) the first four values of ω that lead to singular matrices $\mathbf{D}$ are calculated and plotted in Figure 4 against the values obtained from Eq. (11) of the work by Nordborg [20] (the propagation factor g used in [20] equals $\mathrm{i}kL$). In principle, there are infinitely many frequencies for each wavenumber, corresponding to shorter and shorter wavelength of the beam deflection, but here the focus will be mostly on the lower modes. For higher modes (and frequencies), the cross-section deformation starts playing a role on the rail dynamics, and thus the Euler-Bernoulli beam loses its applicability.

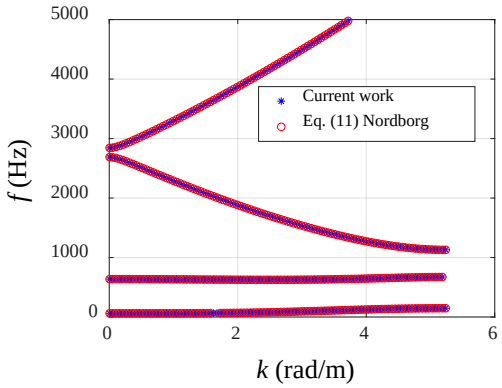

Figure 4. Dispersion lines of the system with ballast as localized spring (current work vs [20]; see digital version of article for coloured figures).

Figure 4 shows a perfect match between the dispersion lines obtained in this work and those obtained with Eq. (11) of Nordborg, which was expected since the system being modelled is exactly the same, even though the derivation differs. This gives a first level of verification to the expressions derived in this work. Figure 4 also shows nicely the existence of stop bands, i.e., frequency ranges at which waves cannot propagate/be sustained. There are two stop bands for this system, one between

150 and 635 Hz, and the other between 672 and 1130 Hz. Stop bands are characteristic of periodic systems.

Figure 5 depicts the four vibration modes of the track for $k = 0$ and $k = 3\,\mathrm{rad/m}$. For $k = 0$, the first mode (Figure 5a) is dominated by the deformation of the ballast springs, the second (Figure 5b) by the deformation of the rail pads and some bending of the rail, and the third and fourth (Figures 5c-d) by the bending of the rail; the third mode presents the largest rail deflection at the connection with the sleeper and at mid-span, while the fourth mode shows the largest deflections at one quarter and three quarters of the span; in both cases, the wavelength corresponds to one sleeper span. At $k = 0$ all dispersion lines show zero slope, meaning that those modes represent standing waves, i.e., the waves do not move to the right nor to the left.

For $k = 3\,\mathrm{rad/m}$, the first mode (Figure 5e) is dominated by the deformation of the ballast spring and by the long wave bending of the rail, the second mode (Figure 5f) is dominated by the deformation of the rail pads and bending of the rail (compared to the first mode, the second mode shows two characteristic wavelengths in the rail deformation while the first mode simply shows one), and the third and fourth modes (Figure 5g-h) represent again the bending of the rails: the wavelength for the third mode is about one-and-a-half sleeper spans, while for the fourth, it is about three quarters of a sleeper span. The slope of the dispersion line of the third mode is negative (Figure 4), meaning that the wave travels to the left (negative group velocity) while the slopes of the other three modes are positive, meaning that the waves travel to the right (positive group velocity).

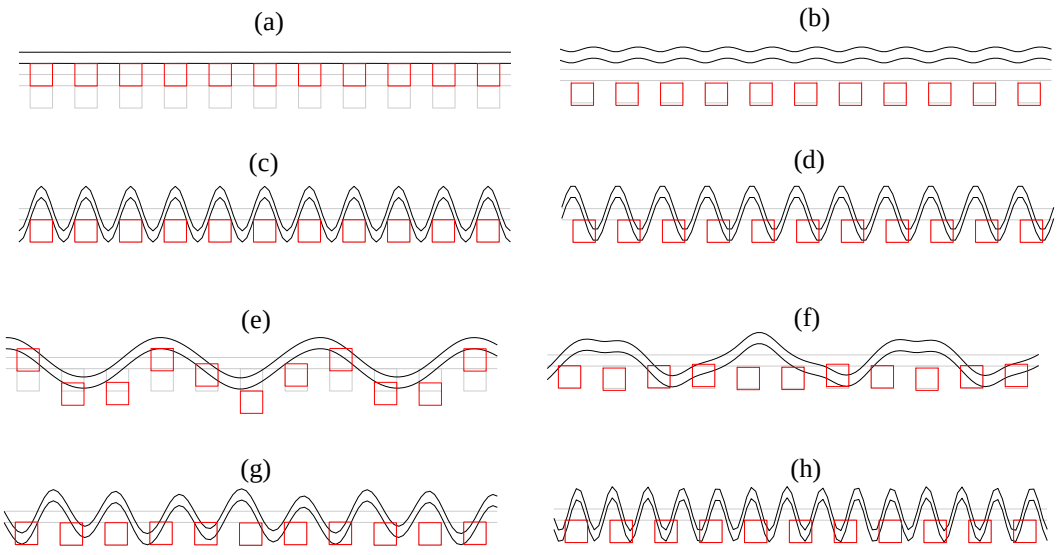

Figure 5. Track modes with ballast as single spring (see digital version of article for coloured figures). (a) first mode for k = 0 rad/m ($f \approx 62$ Hz); (b) second mode for k = 0 rad/m ($f \approx 636$ Hz); (c) third mode for k = 0 rad/m ($f \approx 2690$ Hz); (d) fourth mode for k = 0 rad/m ($f \approx 2840$ Hz); (e) first mode for k = 3 rad/m ($f \approx 93$ Hz); (f) second mode for k = 3 rad/m ($f \approx 627$ Hz); (g) third mode for k = 3 rad/m ($f \approx 1540$ Hz); (h) fourth mode for k = 3 rad/m ($f \approx 4485$ Hz). Download the web material for the time-space representation of these modes.

3.2. Ballast as a lattice

The dispersion lines are now calculated for the case in which the ballast is modelled as a deformable lattice. The under-sleeper pad is assumed 10^3 times stiffer than the ballast, aiming at reproducing an infinite stiffness (in this way, the contact particles move together with the sleepers). A more flexible pad can be used, but since in the reference work no value is provided for the flexibility of the pad (it is condensed in the ballast stiffness), then it is assumed to be rigid.

Regarding the mechanical properties of the ballast, the values $K_{\text{axi}}^{\text{n}}$ and $K_{\text{axi}}^{\text{s}}$ are chosen such that the equivalent static stiffness sensed by an isolated sleeper is $K_{\text{ballast}} = 42.5\times10^6\ \text{N/m}$ and such that the Poisson's ratio of the equivalent 2D continuum (the one that approximates the lattice in the longwave limit [27]) is $\nu = 0.2$. These conditions lead to the following values: $K_{\text{axi}}^{\text{n}} = 3.03\times10^7\ \text{N/m}$ and $K_{\text{axi}}^{\text{s}} = 2.76\times10^6\ \text{N/m}$. The mass m_{b} is calculated assuming an homogenized density of $\rho = 1800\ \text{kg/m}^3$ and a ballast width of $W = 2\ \text{m}$, resulting in $m_{\text{b}} = \rho d^2 W/2 = 4.5\ \text{kg}$ (the model is 2D, and so m_{b} does not represent the mass of a single particle, instead it represents the mass of all particles at any specified height and longitudinal position).

Figure 6 shows three plots of the dispersion lines: the first for all dispersion lines below 5000 Hz, and the second and the third centred around the first two dispersion lines calculated in the previous example. Note in Figure 6a that, when compared to the scenario of Section 3.1, there are two extra dispersion lines for each lattice mass added to the system. These dispersion lines are mostly associated with waves travelling through the lattice, and for the example specified in this section are situated below 1000 Hz. Note also that even though ballast is modelled in a very different way, the dispersion lines associated with the bending of the rail (third and fourth modes of previous example) are not significantly affected.

In Figure 6b, it can be seen that the first dispersion line has a lower cut-off frequency than that of the previous case (red dashed line). This observation is expected because the lattice offers less resistance when all the sleepers are pushed down the same amount (case $k = 0$) than when only one spring is pushed and the others are left free. Recall that the stiffness of the lattice was chosen to match the latter case (i.e., assuming no coupling of the sleepers through ballast, as is the case for ballast modelled as single springs), not the former. In Figure 6c, no dispersion line (blue solid lines) can be directly related to the second mode of the previous case (red dashed line).

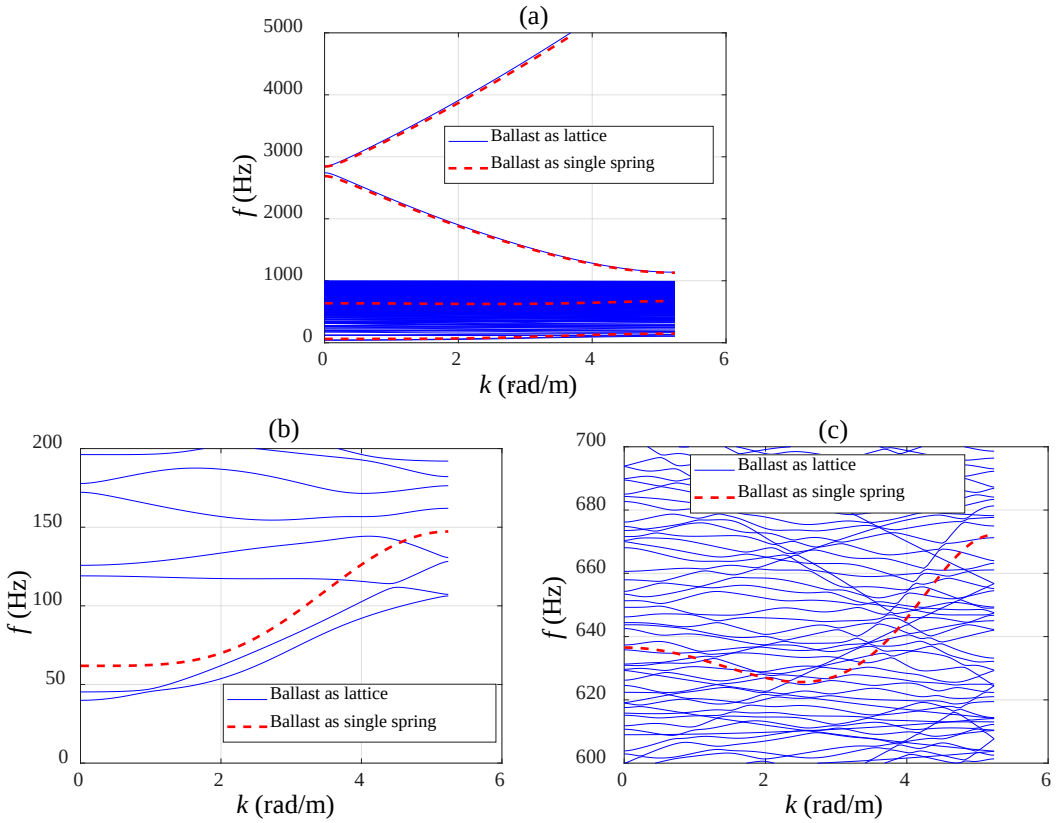

Figure 6. Dispersion lines of the system: ballast as lattice vs ballast as localized spring (see digital version of article for coloured figures). (a) all dispersion lines; (b) zoom-in around first dispersion line of Figure 4; (c) zoom-in around second dispersion line of Figure 4.

Figure 7 shows the first four vibration modes and the modes that correspond to the third and fourth modes of previous example, for $k = 3\,\mathrm{rad/m}$. The first mode (Figure 7a) is similar to the one obtained in Subsection 3.1 (Figure 5e): the rail bends with a similar wavelength and sleepers translate in a similar pattern; in addition, there is a wave travelling on the ballast with the similar wavelength as that of the rail. Despite the similarities, the frequency of the first mode is lower than that of Subsection 3.1, and the reasons for that are the coupling of sleepers by the lattice (that affects the stiffness sensed by the sleepers) and the extra mass that is mobilized due to the waves in the ballast. Regarding the modes 2-4, the second (Figure 7b) is governed mostly by shear waves travelling in the ballast (and causing little bending of the rail, when compared to the previous mode), the third (Figure 7c) by waves travelling in ballast and whose wavelength is half of those in the rail, and the fourth (Figure 7d) by coupled horizontal and vertical motion of the ballast. There is no counterpart of the second, third and fourth modes in the previous example. The modes in Figure 7e-f show a very similar deformation of the rail as those in Figure 5g-h. As in Subsection 3.1, for these modes the ballast remains undeformed, and thus the frequencies are very similar.

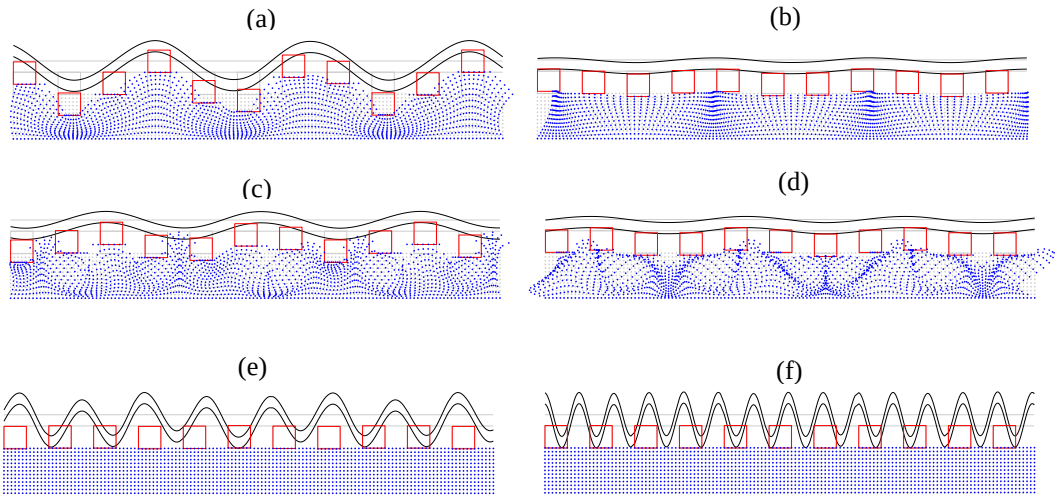

Figure 7. Track modes with ballast as a lattice (see digital version of article for coloured figures). (a) first mode for k = 3 rad/m *(*$f \approx$ 72 Hz*); (b) second mode for* k = 3 rad/m *(*$f \approx$ 81 Hz*); (c) third mode for* k = 3 rad/m *(*$f \approx$ 117 Hz*); (d) fourth mode for* k = 3 rad/m *(*$f \approx$ 139 Hz*); (e) mode corresponding to that of Figure 5g (*$f \approx$ 1556 Hz*); (f) mode corresponding to that of Figure 5h (*$f \approx$ 4530 Hz*). Download the web material for the time-space representation of these modes.*

After comparing the dispersion lines and modes of Sections 3.1 and 3.2 it can be concluded that the features of the rail response are similar in both cases. Nevertheless, modelling ballast as localized springs fails (naturally) to account for the waves that travel through it, and thus is inadequate to study the energy transmission from rails/sleeper to ballast and the mechanisms behind ballast settlement at the particle level.

4. Response due to a moving load – model verification

4.1. Response for moving point force

For the specific case in which the only external excitation is an harmonic force disturbance moving on the rail with constant speed, and assuming that $M_0 = 0$, the vector $\tilde{\mathbf{u}}^{\text{lattice}}(k)$ is null while the vector $\tilde{\mathbf{u}}^{\text{rail}}(k)$ takes the form (see Eq. (41))

$$\tilde{\mathbf{u}}^{\text{rail}}(k) = \frac{F_0}{V\left[\left(\frac{\omega-\omega_0}{V}\right)^4 EI_{\text{rail}} - \omega^2 m_{\text{rail}}\right]} \begin{bmatrix} 1 \\ -\mathrm{i}\frac{\omega-\omega_0}{V} \end{bmatrix} \frac{2\pi}{L} \sum_{h=-\infty}^{+\infty} \delta\left(\frac{\omega-\omega_0}{V} - k - \frac{2\pi h}{L}\right) \tag{56}$$

Due to the presence of the Dirac delta function in $\tilde{\mathbf{u}}^{\text{rail}}(k)$, and therefore in $\tilde{\mathbf{u}}(k)$ and $\tilde{\mathbf{f}}(k)$, the integral (42) sums up to the evaluation of the integrand at point $k = \frac{\omega-\omega_0}{V}$ (for convenience, k_{ref} is set at $k_{\text{ref}} = \frac{\omega-\omega_0}{V}$), i.e., (see also Eq. (25))

$$\mathbf{f}_l = \frac{F_0\, \mathrm{e}^{-\mathrm{i}\frac{\omega-\omega_0}{V}x_l}}{V\left[\left(\frac{\omega-\omega_0}{V}\right)^4 EI_{\mathrm{rail}} - \omega^2 m_{\mathrm{rail}}\right]}\left[\tilde{\mathbf{U}}\left(\frac{\omega-\omega_0}{V}\right)+\mathbf{E}\right]^{-1}\begin{bmatrix}\mathbf{O}_{N\times 1}\\ 1\\ -\mathrm{i}\frac{\omega-\omega_0}{V}\end{bmatrix} \tag{57}$$

The rail pad (F_l and M_l) and under-sleeper pad (F_{ln}^{usp}) forces can thus be evaluated directly without solving numerically any integral, and so can the displacements at the sleepers and at the rails at the sleeper positions. In turn, the response of the rail is again composed of two parts, the part induced by the external force F_0, given by (Eqs. (45)-(46) with $M_0 = 0$)

$$\begin{bmatrix} u_{F_0}^{\mathrm{rail}}(x)\\ \theta_{F_0}^{\mathrm{rail}}(x)\end{bmatrix} = \frac{F_0\, \mathrm{e}^{-\mathrm{i}\frac{\omega-\omega_0}{V}x}}{V\left[\left(\frac{\omega-\omega_0}{V}\right)^4 EI_{\mathrm{rail}} - \omega^2 m_{\mathrm{rail}}\right]}\begin{bmatrix}1\\ -\mathrm{i}\frac{\omega-\omega_0}{V}\end{bmatrix} \tag{58}$$

$$\begin{bmatrix} M_{F_0}^{\mathrm{rail}}(x)\\ V_{F_0}^{\mathrm{rail}}(x)\end{bmatrix} = \frac{F_0\, \mathrm{e}^{-\mathrm{i}\frac{\omega-\omega_0}{V}x}}{V\left[\left(\frac{\omega-\omega_0}{V}\right)^4 EI_{\mathrm{rail}} - \omega^2 m_{\mathrm{rail}}\right]}\begin{bmatrix}-\left(\frac{\omega-\omega_0}{V}\right)^2\\ \mathrm{i}\left(\frac{\omega-\omega_0}{V}\right)^3\end{bmatrix} \tag{59}$$

and the part induced by the rail pad forces, which is the evaluation of integrals (49)-(50) taking into account the presence of the Dirac delta function:

$$\begin{bmatrix} u_{\mathrm{rp}}^{\mathrm{rail}}(x)\\ \theta_{\mathrm{rp}}^{\mathrm{rail}}(x)\end{bmatrix} = -\frac{1}{4EI_{\mathrm{rail}}}\begin{bmatrix} \frac{-\mathrm{i}\,c\left(\mathrm{i}\bar{k},\frac{\omega-\omega_0}{V},-x\right)-c\left(\bar{k},\frac{\omega-\omega_0}{V},-x\right)}{\bar{k}^3} & \frac{d\left(\mathrm{i}\bar{k},\frac{\omega-\omega_0}{V},-x\right)-d\left(\bar{k},\frac{\omega-\omega_0}{V},-x\right)}{\bar{k}^2}\\ \frac{-d\left(\mathrm{i}\bar{k},\frac{\omega-\omega_0}{V},-x\right)+d\left(\bar{k},\frac{\omega-\omega_0}{V},-x\right)}{\bar{k}^2} & \frac{-\mathrm{i}c\left(\mathrm{i}\bar{k},\frac{\omega-\omega_0}{V},-x\right)+c\left(\bar{k},\frac{\omega-\omega_0}{V},-x\right)}{\bar{k}}\end{bmatrix}\begin{bmatrix}\tilde{f}\\ \tilde{m}\end{bmatrix} \tag{60}$$

$$\begin{bmatrix} M_{\mathrm{rp}}^{\mathrm{rail}}(x)\\ V_{\mathrm{rp}}^{\mathrm{rail}}(x)\end{bmatrix} = -\frac{\bar{k}^2}{4}\begin{bmatrix} \frac{\mathrm{i}\,c\left(\mathrm{i}\bar{k},\frac{\omega-\omega_0}{V},-x\right)-c\left(\bar{k},\frac{\omega-\omega_0}{V},-x\right)}{\bar{k}^3} & \frac{-d\left(\mathrm{i}\bar{k},\frac{\omega-\omega_0}{V},-x\right)-d\left(\bar{k},\frac{\omega-\omega_0}{V},-x\right)}{\bar{k}^2}\\ \frac{d\left(\mathrm{i}\bar{k},\frac{\omega-\omega_0}{V},-x\right)+d\left(\bar{k},\frac{\omega-\omega_0}{V},-x\right)}{\bar{k}^2} & \frac{\mathrm{i}\,c\left(\mathrm{i}\bar{k},\frac{\omega-\omega_0}{V},-x\right)+c\left(\bar{k},\frac{\omega-\omega_0}{V},-x\right)}{\bar{k}}\end{bmatrix}\begin{bmatrix}\tilde{f}\\ \tilde{m}\end{bmatrix} \tag{61}$$

with

$$\begin{bmatrix}\tilde{f}\\ \tilde{m}\end{bmatrix} = \frac{F_0}{V\left[\left(\frac{\omega-\omega_0}{V}\right)^4 EI_{\mathrm{rail}} - \omega^2 m_{\mathrm{rail}}\right]}\begin{bmatrix}\mathbf{O}_{N\times 2}\\ 1 \quad 0\\ 0 \quad 1\end{bmatrix}^{\mathrm{T}}\left[\tilde{\mathbf{U}}\left(\frac{\omega-\omega_0}{V}\right)+\mathbf{E}\right]^{-1}\begin{bmatrix}\mathbf{O}_{N\times 1}\\ 1\\ -\mathrm{i}\frac{\omega-\omega_0}{V}\end{bmatrix} \tag{62}$$

For the calculation of the response of any mass of the lattice, the contribution of external forces is null (no external forces at the lattice), while integral (52) can be simplified to

$$u_{\alpha,i,j}^{\mathrm{usp}} = \frac{d\, F_0}{L\, V\left[\left(\frac{\omega-\omega_0}{V}\right)^4 EI_{\mathrm{rail}} - \omega^2 m_{\mathrm{rail}}\right]}\sum_{m=0}^{N+M-1}\tilde{f}_{m,i}^{\mathrm{usp}}\,\bar{u}_{\alpha z,j,0}^{*}\left(\frac{\omega-\omega_0}{V}-\frac{2\pi m}{L}\right) \tag{63}$$

where (see also Eq. (54))

$$\tilde{f}_{m,i}^{\text{usp}} = \begin{bmatrix} \left\{ \mathrm{e}^{\mathrm{i}\left(\frac{\omega-\omega_0}{V} - \frac{2\pi m}{L}\right)\overrightarrow{(n-i)\,d}} \right\} & 0 & 0 \end{bmatrix} \left[\tilde{\mathbf{U}}\left(\frac{\omega-\omega_0}{V}\right) + \mathbf{E} \right]^{-1} \begin{bmatrix} \mathbf{O}_{N\times 1} \\ 1 \\ -\mathrm{i}\frac{\omega-\omega_0}{V} \end{bmatrix} \tag{64}$$

The summation over m in Eq. (63) results from the fact that the periodicity of the lattice is $N+M$ times smaller than the periodicity of the sleepers (of the assembled structure). Thus, when assessing integral (52), $N+M$ Dirac functions are found within the region of integration.

4.2. Time domain response

In the previous subsection the frequency domain response of all components has been given. The time domain response can be obtained afterwards by applying the inverse Fourier transform. That is, if $\tilde{f}(\omega)$ represents any of the variables described earlier (translation, rotation, force, etc.), then its time domain counterpart $f(t)$ is calculated with

$$f(t) = \frac{1}{2\pi}\int_{-\infty}^{+\infty} \tilde{f}(\omega)\mathrm{e}^{\mathrm{i}\omega t}\mathrm{d}\omega \tag{65}$$

For most cases, the analytical evaluation of integral (65) is impossible. The use of Fast Fourier transform techniques is, for these cases, the preferred option. An inspection of all the frequency domain variables reveals that all contain one or multiple exponents of the type $\exp\left(-\mathrm{i}\frac{\omega-\omega_0}{V}\overline{x}\right)$ where $\overline{x}$ is a measure of the longitudinal position. This exponent reflects the moving nature of the load, and when transformed to time, results in steady-state deformation pattern that moves with the load and oscillates with frequency ω_0. This property allows calculating the time-space responses in an efficient manner, in the sense that the inverse Fourier transform only needs to be calculated for the time shifted variable $\tau = t - \overline{x}/V$, and not for each position of the sleeper/rail/lattice mass.

4.3. Verification

To verify the equations derived in this paper, the results obtained from evaluating expressions (56)-(64) are compared with those obtained with a time-space domain method. The track properties are the same as defined in Section 3.2, but with a couple of changes: the sleepers are free to rotate and have rotational inertia $J_{\mathrm{s}} = 3.75\ \mathrm{kg.m}^2$; the rotational stiffness of the rail pads is $K_\theta = 11.25\times10^6\ \mathrm{N.m}$; a small amount of stiffness proportional damping is added to the rail and the lattice by means of complex stiffnesses of the type $\overline{EI}_{\mathrm{rail}} = EI_{\mathrm{rail}}(1+\eta\omega\mathrm{i})$, $\overline{K}^{\mathrm{n}}_{\mathrm{axi}} = K^{\mathrm{n}}_{\mathrm{axi}}(1+\eta\omega\mathrm{i})$ and $\overline{K}^{\mathrm{s}}_{\mathrm{axi}} = K^{\mathrm{s}}_{\mathrm{axi}}(1+\eta\omega\mathrm{i})$, where the damping factor is $\eta = 0.002\ \mathrm{s}$. The amount of damping considered in the ballast is of the same order of that considered in [20] ($\eta \approx C_{\mathrm{Ballast}}/K_{\mathrm{Ballast}}$). For the calculation of the inverse Fourier transform, 10001 equally spaced frequencies between 0 and 1000 Hz are considered.

The time-space domain model is based on standard Finite Elements for the rail and lumped masses for sleepers and lattice. The model is made long enough so that the transient effects (entrance of the load) and reflection effects (at the fictitious boundaries) do not pollute the response of the system. A sensitivity analysis revealed that 300 sleepers are enough to suppress these effects.

The Newmark integration algorithm with a time step of 0.0002 s is used to solve system of the second order differential equations in time.

The results to be compared are the time dependent vertical displacements of the rail at the connection with the mid sleeper and the time dependent horizontal displacements of the ballast particle at column $i = 0$ and row $j = 6$ (mid height of ballast). The external force is of the type $F(x,t) = F_0 \cos(\omega_0 t)\delta(x - Vt)$. For comparison purposes, the response of the rail obtained with the lumped ballast model of Section 3 (no rotation of sleepers, equivalent to Nordborg [20]) is also shown.

Three excitation scenarios are considered, all with $F_0 = 1$ (the formulation is linear, so it suffices to analyse a unit amplitude loading): i) $V = 60\ \mathrm{m/s}$ ($\approx 220\mathrm{km/h}$) and $\omega_0 = 0$, which is representative of the gravitational load induced by an intercity train travelling at operational speed in some countries; ii) $V = 60\ \mathrm{m/s}$ and $\omega_0 = 628\ \mathrm{rad/s}$ ($\approx 100\ \mathrm{Hz} = V/L$), which is representative of the excitation due to the sleeper periodicity; iii) $V = 400\ \mathrm{m/s}$ and $\omega_0 = 0$, which represents an unrealistic scenario but is shown nonetheless to verify that the model provides the correct results in the supersonic case. Figure 8 shows the rail and the ballast responses obtained for these excitation parameters.

For the first loading scenario, the vertical deflection of the rail (Figure 8a) is nearly symmetric (the response is practically mirrored at $t = 0$, which is the moment that the load crosses the section under analyses), while the longitudinal motion of the ballast (Figure 8b) is anti-symmetric. These features are typical of systems excited by constant forces moving at speeds lower than the minimum phase velocity of free waves, as discussed in Section 3. For the second scenario (Figure 8c,d), the load speed is still below the minimum phase velocity, but the oscillatory nature of the excitation causes the frequency of the response to be higher before the load passes than after that (Doppler effect). In turn, in the third scenario (Figure 8e,f), because the load moves at a speed higher than the minimum phase velocity (supersonic case), the response is practically zero before the load arrives, increases sharply when the load is passing, and decays after the load has passed.

In all three loading scenarios, the results obtained with the expressions derived in this work (blue solid lines) match very well with those obtained with the numerical approach (red dashed lines), which verifies the correctness of the expressions. Regarding the rail response obtained with the equivalent lumped model for the ballast (dotted black lines), it can be observed that it differs from the other two in all three loading scenarios: in the first scenario (Figure 8a), the time evolution is very similar, but the maximum response is slightly smaller; in the second scenario (Figure 8c), the main trends of the time response seem to match, but the amplitudes of the peaks are larger; in the third scenario (Figure 8e), the rail response attenuates faster. The mismatch in the results is naturally explained by the different levels of detail employed in the description of the ballast. These differences support the need of more detailed models for the correct assessment of the dynamic behaviour of the track, even for cases in which only the dynamic response of the rail is of interest.

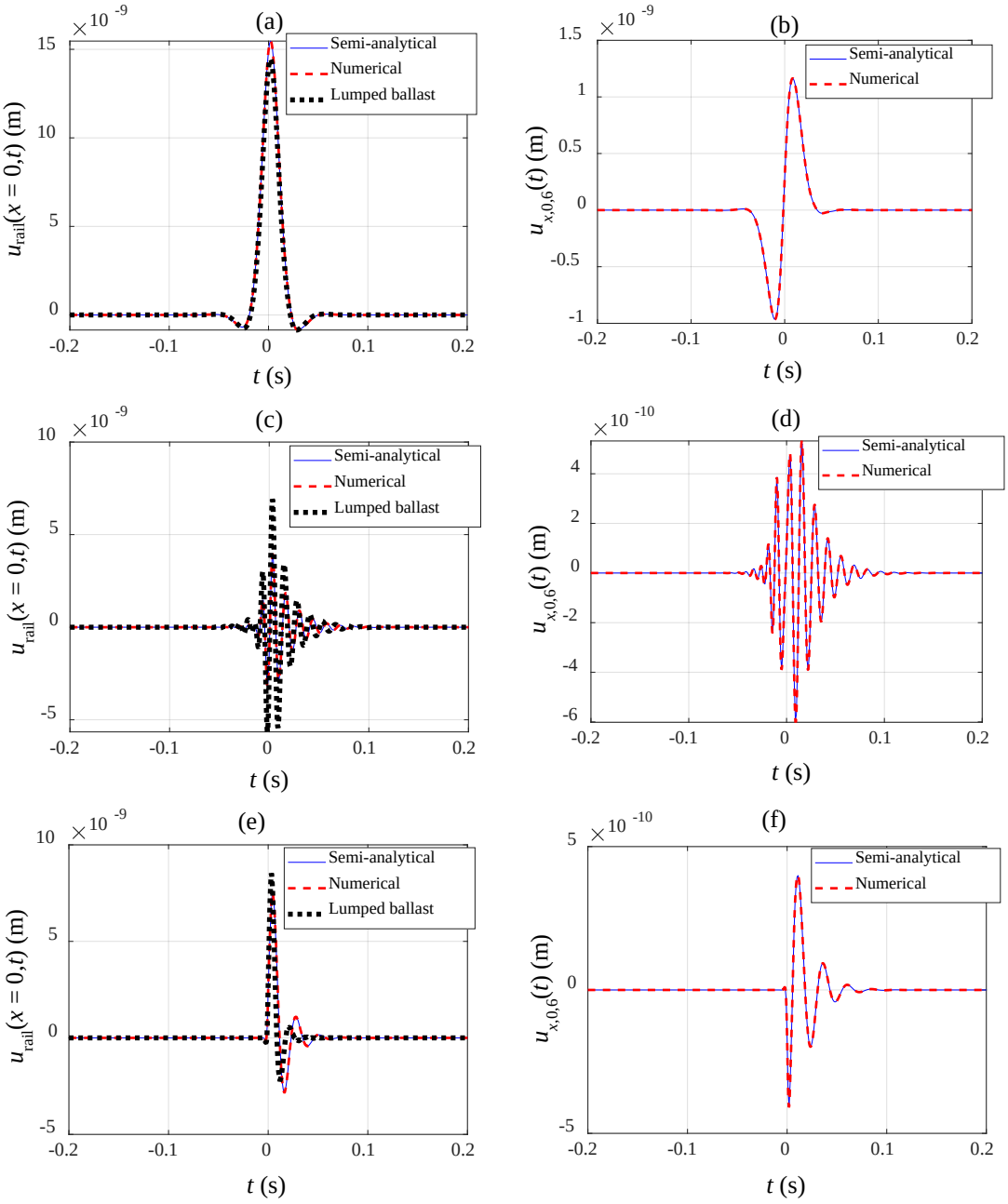

Figure 8. Vertical displacements of the rail (a,c,e) and horizontal displacement of the ballast (b,d,f) for different loading scenarios (see digital version of article for coloured figures). (a,b) V = 60 m/s, ω_0 = 0 rad/s; (c,d) V = 60 m/s, ω_0 = 628 rad/s; (e,f) V = 400 m/s, ω_0 = 0 rad/s.

5. Analysis of lattice response and critical speeds

As mentioned in the beginning of Section 2, the model proposed in this work is an extension of the work by Suiker and collaborators [26,27] in the sense that sleepers and rails are incorporated. Suiker and collaborators' model, which only considers a lattice layer, has been used to analyse the lattice response and assess the critical velocities of the system, and the following conclusions have been reached (for constant moving loads and low viscous damping in the lattice): i) the response of the lattice induced by forces moving at low speed is less local than that for forces moving at higher speed; ii) for large particle diameters d, there is a critical speed much lower than the minimum

phase velocity of the free waves of the lattice layer (which the authors termed “Rayleigh wave”). Whether these observations remain valid when the track is added to the ballast layer is a question that still remains. The present section answers this question by means of comparing the responses of an isolated lattice layer to that of the model proposed here, when both are acted upon by constant moving loads.

In order to achieve a viscosity in the same order of magnitude as the one considered in [26], the damping factor is reduced to $\eta = 1.2 \times 10^{-5}\ \mathrm{s}$, rendering the system practically undamped[3]. For this reason, the contributions of higher harmonics cannot be disregarded, and thus the inverse Fourier transform is calculated, in this section, for 10001 frequencies ranging from 0 and 10000Hz.

To verify the conclusion about the steady-state response of the lattice, the vertical displacements at row $j = 2$ (third row of particles from the top, at the depth $2d = 0.1\ \mathrm{m}$) are calculated for a vertical force moving on the rail at the speeds $V = 28\ \mathrm{m/s}\ \ (\approx 100\ \mathrm{km/h})$, $V = 56\ \mathrm{m/s}\ \ (\approx 200\ \mathrm{km/h})$, $V = 84\ \mathrm{m/s}\ \ (\approx 300\ \mathrm{km/h})$ and $V = 98\ \mathrm{m/s}\ \ (\approx 350\ \mathrm{km/h})$ and compared with those obtained when sleepers and rails are removed and the load is applied directly at the surface of the ballast (equations from [26]). The results are depicted in Figure 9.

The blue solid lines in Figure 9 are in accordance with the findings of Suiker and collaborators: as the load speeds increases from 100 km/h to 300 km/h, the length of the disturbed wake behind the load is shorter and shorter, thus confirming that for lower speed the response is less local. However, for the speed 350 km/h, the wake behind the load broadens again, while the disturbance in front of the load shortens. The reason for this finding is that at 350 km/h the load moves at a supersonic speed, and thus there is strong radiation of waves behind the load. Suiker and collaborators did not report this case because they only analysed subsonic scenarios (the highest speed they considered was 500 km/h, while the minimum phase velocity of the system was around 700 km/h; in this work, the minimum phase velocity of the lattice is around 325 km/h).

Regarding the red dashed lines in Figure 9, corresponding to the full model, it is observed that increasing the load speed does not change significantly the vertical response of the ballast, neither in terms of shape nor in terms of amplitude. This suggests that the load speed is still below the first critical speed of the system, and also shows that the finding of Suiker and collaborators (that lower load speeds do lead to less local responses) no longer applies when the rails and sleepers are added to the model.

[3] The damping considered here is unrealistically low. Such value is solely used to verify whether the conclusions obtained in work [26], for the case of very low damping in the ballast, are still applicable. Nevertheless, for the current model, a more realistic value of damping (100 times larger) would yield very similar results: the asymmetry of the response with respect to the loaded point would be more pronounced than in Figure 9 (due to the effect of damping), but the main features of the response would remain.

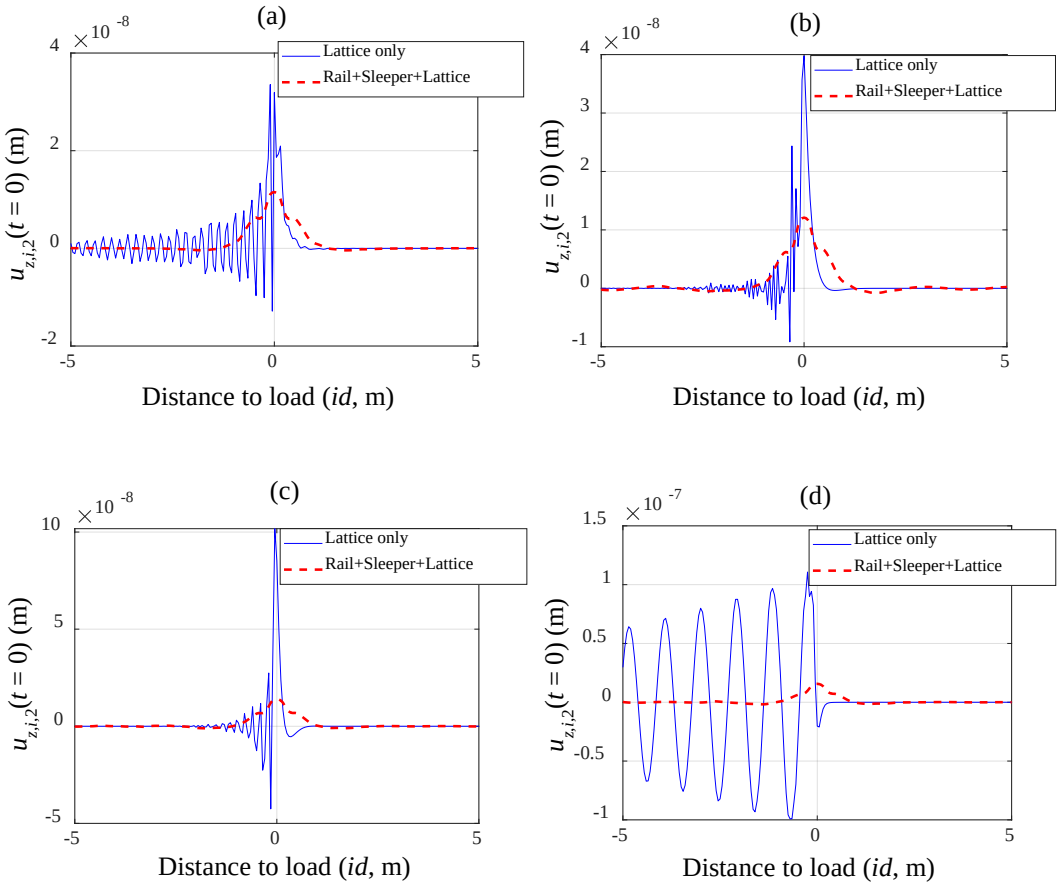

Figure 9. Vertical displacements of the ballast when considering only lattice (blue solid lines) and when considering the full track model (red dashed lines) for varying load speed (see digital version of article for coloured figures). (a) V = 28 m/s (100 km/h); (b) V = 28 m/s (200 km/h); (c) V = 84 m/s (300 km/h); (d) V = 98 m/s (350 km/h).

To examine how the ballast behaves when a full track is considered and as the load speed keeps increasing and exceeds the minimum phase velocity, the vertical response of the lattice at row $j = 2$ is calculated for load speeds ranging up to 1500 km/h. Figure 10 shows the results. It can be seen that there is a transition in the shape of the ballast response when the load speed steps up from 350km/h to 500km/h: for the latter speed, the maximum deflection is still under the load but the steady-state pattern is no longer quasi symmetric; instead it is predominant behind the load, suggesting that the minimum phase speed of free waves in the track is being approached (in accordance with Figure 11). Also, the wake behind the load is characterized by a dominant wavelength, a feature similar to that reported in Figure 9 for the lattice only (lower right panel, blue line). As the load speed keeps increasing, the deformation pattern in the wake of the load further changes, showing longer wavelengths for higher load speeds. The deformation pattern in front of the load narrows (even) further, suggesting that the critical speed has been far exceeded.

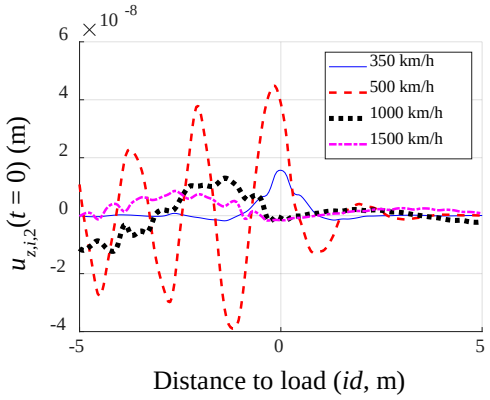

Figure 10. Vertical displacements of the ballast when considering the full track model for varying load speed (see digital version of article for coloured figures).

The existence of a critical speed much lower than the minimum phase velocity of the system is investigated by calculating the maximum vertical displacement of the ballast (again at the depth $2d = 0.1\,\mathrm{m}$) for speeds ranging from 1 km/h to 600 km/h. The dependence of the maximum displacement on the load speed is plotted in Figure 11. The blue solid line reveals that there is indeed a very low load speed (for the parameters used there are actually two, one near 3 km/h and another near 10 km/h) that induces an amplified response. However, this is not observed when the rails and sleepers are considered (red dashed line). The reason for this difference lies, in the authors' view, in how the load is defined in both cases: while in work [26] the load is a succession of Dirac impulses, each applied at a different particle and at a different time instant, in the model proposed here the load is continuously transmitted to the lattice via the sleepers; also, in the first scenario, the time difference between each impulse increases as the load speed decreases (it takes longer for the load to move from one particle to the following), potentially accentuating the transient response due to the impact. In addition to the suppression of these lower critical speeds, the inclusion of the rails and sleepers increases the minimum phase velocity of the track, in this case from 325 km/h to 530 km/h. These differences highlight the need of considering full track models even if the focus of study is on the foundation.

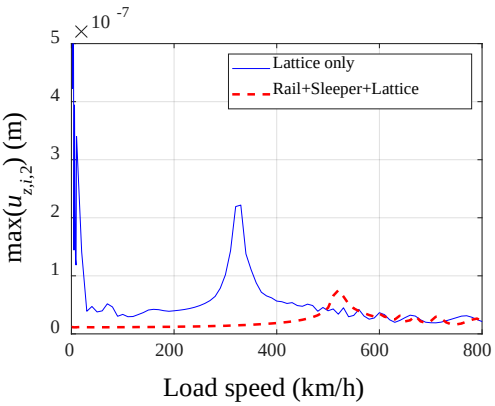

Figure 11. Maximum vertical displacement of ballast as function of load speed. Blue solid line: lattice only. Red dashed line: lattice + rails +sleepers (see digital version of article for coloured figures).

6. Final considerations

This paper proposes a model for ballasted railway tracks in which ballast is modelled as a lattice, i.e., a regular network of discrete masses connected by (visco)elastic elements. A solution procedure is presented in which the periodic geometry of the system is employed in order to obtain the frequency domain response of the system in terms of an inverse Fourier integral/transform. The solution procedure is verified by comparing the responses thus obtained with the responses obtained with a space-time solution procedure, and a perfect match is observed.

The model is also used to assess the natural modes of vibration of the track and compare them to those of a track in which ballast is lumped into discretized elastic connections, a simplification used often in the literature. It is observed that the two models give similar natural shapes for the rails, and that the simpler model fails to capture the modes in which the energy is concentrated in the ballast. This is obviously not surprising since the simpler model condenses all the ballast degrees of freedom into the ones right below the sleepers.

The model is further used to assess the critical speeds of the track and to verify the observations from a similar work in which ballast is also modelled as a lattice, but in which the superstructure (sleepers and rails) is disregarded. It is observed that adding rails and sleepers considerably increases the minimum phase velocity of the system, and also that it cancels the very low critical speed observed in the mentioned work. Additionally, for subsonic excitations, adding the superstructure changes the response of the lattice from being mostly concentrated in the wake of load to a practically symmetric steady-state deformation pattern moving with the load. These differences point out the need of adding the superstructure even for the cases in which only the foundation response is of interest.

As a final remark, it must be mentioned that even though the model presented here is linear, it is in the authors' plans to replace the connections between particles by nonlinear connections defined in such a way that the non-recoverable settling behaviour of the ballast is reproducible. The present work thus serves as a launching framework for that task, which will be tackled and reported in a future work. Regardless of that, it is appropriate to note that despite not being the main motivation for this work, the model here presented can very well be used to asses main features of railway tracks, such as critical speeds, energy propagations, vehicle-track interaction, etc..

Acknowledgments

This research is supported by the Dutch Technology Foundation TTW (Project 15968), part of the Netherlands Organisation for Scientific Research (NWO), and which is partly funded by the Ministry of Economic Affairs.

Appendix A - Wavenumber solution of a layered lattice

In this appendix, it is explained how to calculate the wavenumber Green's functions of a layered lattice. First the equations of motion of one layer are presented and the corresponding homogeneous solutions are obtained. Then, the boundary equations are solved based on the homogeneous solutions, and after elimination of common variables, the stiffness matrix that relates

surface forces with surface displacements (of one layer) is obtained. Finally the stiffness matrices of all layers are assembled, and from the assembled system the layered lattice can be solved for the exterior forces. Despite the fact that in the main body of the paper only a single layer is considered, the solution procedure is explained for layered lattices to make the problem generic, which allows studying the influence of subgrade (sub-ballast and soil).

The lattice type considered in this work is as depicted in Figure 2, with the diagonal springs being written as a combination of the non-diagonal longitudinal and shear springs: $K^{\mathrm{n}}_{\mathrm{diag}} = \left(K^{\mathrm{n}}_{\mathrm{axi}} - K^{\mathrm{s}}_{\mathrm{axi}}\right)\!/2$. The mass of each particle is m_{b}. This lattice type is as proposed in the work by Suiker et al. [26,27]. Different lattices types (for example, honeycomb lattices [32]) may require a slightly different solution methods, which are not addressed in this work.

A.1 – Equations of motion and solution type for masses inside a layer of the lattice

For a lattice layer that is free of any load in its interior, the equations of motion for a mass inside the layer (at column i and row j) are

$$\begin{cases} -\omega^2 m_{\mathrm{b}} u_{x,i,j} + K^{\mathrm{n}}_{\mathrm{axi}}\left(2u_{x,i,j} - u_{x,i-1,j} - u_{x,i+1,j}\right) + K^{\mathrm{s}}_{\mathrm{axi}}\left(2u_{x,i,j} - u_{x,i,j-1} - u_{x,i,j+1}\right) \\ \qquad + \tfrac{1}{2} K^{\mathrm{n}}_{\mathrm{diag}}\left(4u_{x,i,j} - u_{x,i-1,j-1} - u_{x,i+1,j-1} - u_{x,i+1,j+1} - u_{x,i-1,j+1}\right) \\ \qquad + \tfrac{1}{2} K^{\mathrm{n}}_{\mathrm{diag}}\left(4u_{z,i,j} - u_{z,i-1,j-1} - u_{z,i+1,j-1} - u_{z,i+1,j+1} - u_{z,i-1,j+1}\right) = 0 \\ \\ -\omega^2 m_{\mathrm{b}} u_{z,i,j} + K^{\mathrm{s}}_{\mathrm{axi}}\left(2u_{z,i,j} - u_{z,i-1,j} - u_{z,i+1,j}\right) + K^{\mathrm{n}}_{axi}\left(2u_{z,i,j} - u_{z,i,j-1} - u_{z,i,j+1}\right) \\ \qquad + \tfrac{1}{2} K^{\mathrm{n}}_{\mathrm{diag}}\left(4u_{z,i,j} - u_{z,i-1,j-1} - u_{z,i+1,j-1} - u_{z,i+1,j+1} - u_{z,i-1,j+1}\right) \\ \qquad + \tfrac{1}{2} K^{\mathrm{n}}_{\mathrm{diag}}\left(4u_{x,i,j} - u_{x,i-1,j-1} - u_{x,i+1,j-1} - u_{x,i+1,j+1} - u_{x,i-1,j+1}\right) = 0 \end{cases} \tag{A.1}$$

which accept solutions of the type

$$\begin{bmatrix} u_{x,i,j} \\ u_{z,i,j} \end{bmatrix} = \mathrm{e}^{-\mathrm{i}(\kappa i + \kappa_z j)d} \begin{bmatrix} A_x \\ A_z \end{bmatrix} \tag{A.2}$$

where A_x and A_z are amplitudes of oscillations in the horizontal and vertical directions, κ is the horizontal wavenumber and κ_z is the vertical wavenumber. For a given pair (κ, ω), the solutions of the type (A.2) are found by solving for κ_z, A_x and A_z the following eigenvalue problem

$$\begin{bmatrix} k_{11} & k_{12} \\ k_{21} & k_{22} \end{bmatrix} \begin{bmatrix} A_x \\ A_z \end{bmatrix} = \begin{bmatrix} 0 \\ 0 \end{bmatrix} \tag{A.3}$$

where

$$
\begin{aligned}
k_{11} &= \bar{K}_1 - \omega^2 m_\mathrm{b} - 2\left(K^\mathrm{n}_\mathrm{axi}\cos\left(\kappa d\right) + K^\mathrm{s}_\mathrm{axi}\cos\left(\kappa_z d\right)\right) - \bar{K}_2\left(\kappa_z\right) \\
k_{12} &= k_{21} = K^\mathrm{n}_\mathrm{diag}\left(\cos\left(\kappa d + \kappa_z d\right) + \cos\left(\kappa d - \kappa_z d\right)\right) \\
k_{22} &= \bar{K}_1 - \omega^2 m_\mathrm{b} - 2\left(K^\mathrm{n}_\mathrm{axi}\cos\left(\kappa_z d\right) + K^\mathrm{s}_\mathrm{axi}\cos\left(\kappa d\right)\right) - \bar{K}_2\left(\kappa_z\right) \\
\bar{K}_1 &= 2\left(K^\mathrm{n}_\mathrm{axi} + K^\mathrm{s}_\mathrm{axi} + K^\mathrm{n}_\mathrm{diag}\right) \\
\bar{K}_2\left(\kappa_z\right) &= K^\mathrm{n}_\mathrm{diag}\left(\cos\left(\kappa d + \kappa_z d\right) + \cos\left(\kappa d - \kappa_z d\right)\right)
\end{aligned}
\tag{A.4}
$$

The eigenvalue problem (A.3) contains four distinct solutions,

$$
\begin{aligned}
\kappa_{z1} &= \frac{1}{d}\operatorname{acos}\left(\frac{\omega^2 m_\mathrm{b} + K^\mathrm{n}_\mathrm{axi}\left(\cos\left(\kappa d\right) - 4\right) + K^\mathrm{s}_\mathrm{axi}\cos\left(\kappa d\right)}{K^\mathrm{s}_\mathrm{axi}\left(1 - 2\cos\left(\kappa d\right)\right) + K^\mathrm{n}_\mathrm{axi}\left(1 + 2\cos\left(\kappa d\right)\right)}\right) \\
\kappa_{z2} &= \frac{1}{d}\operatorname{acos}\left(\frac{\omega^2 m_\mathrm{b} + K^\mathrm{n}_\mathrm{axi}\left(\cos\left(\kappa d\right) - 2\right) + K^\mathrm{s}_\mathrm{axi}\left(\cos\left(\kappa d\right) - 2\right)}{K^\mathrm{s}_\mathrm{axi} + K^\mathrm{n}_\mathrm{axi}}\right) \\
\kappa_{z3} &= -\frac{1}{d}\operatorname{acos}\left(\frac{\omega^2 m_\mathrm{b} + K^\mathrm{n}_\mathrm{axi}\left(\cos\left(\kappa d\right) - 4\right) + K^\mathrm{s}_\mathrm{axi}\cos\left(\kappa d\right)}{K^\mathrm{s}_\mathrm{axi}\left(1 - 2\cos\left(\kappa d\right)\right) + K^\mathrm{n}_\mathrm{axi}\left(1 + 2\cos\left(\kappa d\right)\right)}\right) \\
\kappa_{z4} &= -\frac{1}{d}\operatorname{acos}\left(\frac{\omega^2 m_\mathrm{b} + K^\mathrm{n}_\mathrm{axi}\left(\cos\left(\kappa d\right) - 2\right) + K^\mathrm{s}_\mathrm{axi}\left(\cos\left(\kappa d\right) - 2\right)}{K^\mathrm{s}_\mathrm{axi} + K^\mathrm{n}_\mathrm{axi}}\right)
\end{aligned}
\tag{A.5}
$$

whose corresponding eigenvectors $\left\{A_{xl}, A_{zl}\right\}^\mathrm{T}$ are (do not confound l used here to describe the eigenpair number with the same letter used in the main body of the paper to describe the sleeper number)

$$
\begin{aligned}
A_{xl} &= 1 \\
A_{zl} &= \frac{\bar{K}_1 - \omega^2 m_b - 2\left(K^\mathrm{n}_\mathrm{axi}\cos\left(\kappa d\right) + K^\mathrm{s}_\mathrm{axi}\cos\left(\kappa_{zl} d\right)\right) - \bar{K}_2\left(\kappa_{zl}\right)}{\bar{K}_2\left(\kappa_{zl}\right)}
\end{aligned}
\tag{A.6}
$$

Hence, the displacements $u_{\alpha,i,j}$ at any point of the lattice can be rewritten in terms of these eigenpairs and unknown modal amplitudes A_l as

$$
\begin{bmatrix} u_{x,i,j} \\ u_{z,i,j} \end{bmatrix} = \mathrm{e}^{\mathrm{i}\left(\omega t - \kappa\, id\right)} \begin{bmatrix} A_{x1}\mathrm{e}^{-\mathrm{i}\kappa_{z1} jd} & A_{x2}\mathrm{e}^{-\mathrm{i}\kappa_{z2} jd} & A_{x3}\mathrm{e}^{-\mathrm{i}\kappa_{z3} jd} & A_{x4}\mathrm{e}^{-\mathrm{i}\kappa_{z4} jd} \\ A_{z1}\mathrm{e}^{-\mathrm{i}\kappa_{z1} jd} & A_{z2}\mathrm{e}^{-\mathrm{i}\kappa_{z2} jd} & A_{z3}\mathrm{e}^{-\mathrm{i}\kappa_{z3} jd} & A_{z4}\mathrm{e}^{-\mathrm{i}\kappa_{z4} jd} \end{bmatrix} \begin{bmatrix} A_1 \\ A_2 \\ A_3 \\ A_4 \end{bmatrix}
\tag{A.7}
$$

The modal amplitudes A_l must be calculated such that the boundary conditions at the top and bottom of the lattice layer are satisfied.

A.2 – Equation for masses at the upper and lower surfaces of the layer

The motion of a mass at the upper boundary ($j = 0$) of a layer of the lattice is governed by the pair of equations

$$\begin{cases} -\boxed{\tfrac{1}{2}}\omega^2 m_{\mathrm{b}} u_{x,i,0} + \boxed{\tfrac{1}{2}} K^{\mathrm{n}}_{\mathrm{axi}} \left(2u_{x,i,0} - u_{x,i-1,0} - u_{x,i+1,0}\right) + K^{\mathrm{s}}_{\mathrm{axi}} \left(u_{x,i,0} - u_{x,i,1}\right) \\ \qquad + \tfrac{1}{2} K^{\mathrm{n}}_{\mathrm{diag}} \left(2u_{x,i,0} - u_{x,i+1,1} - u_{x,i-1,1}\right) + \tfrac{1}{2} K^{\mathrm{n}}_{\mathrm{diag}} \left(2u_{z,i,0} - u_{z,i+1,1} - u_{z,i-1,1}\right) = F_{x,i,0} \\ -\boxed{\tfrac{1}{2}}\omega^2 m_{b} u_{z,i,0} + \boxed{\tfrac{1}{2}} K^{\mathrm{s}}_{\mathrm{axi}} \left(2u_{z,i,0} - u_{z,i-1,0} - u_{z,i+1,0}\right) + K^{\mathrm{n}}_{\mathrm{axi}} \left(u_{z,i,j} - u_{z,i,1}\right) \\ \qquad + \tfrac{1}{2} K^{\mathrm{n}}_{\mathrm{diag}} \left(2u_{z,i,j} - u_{z,i+1,1} - u_{z,i-1,1}\right) + \tfrac{1}{2} K^{\mathrm{n}}_{\mathrm{diag}} \left(2u_{x,i,j} - u_{x,i+1,1} - u_{x,i-1,1}\right) = F_{z,i,0} \end{cases} \tag{A.8}$$

where $F_{x,i,0}$ and $F_{z,i,0}$ are the externally applied forces at the upper boundary. Likewise, the motion of a mass at the lower boundary ($j = N$; do not confound N used here to describe the depth of the last particle with the same letter used in the main body of the paper to describe the number of particles in contact with the sleepers) of a layer of the lattice is governed by the pair of equations

$$\begin{cases} -\boxed{\tfrac{1}{2}}\omega^2 m_{\mathrm{b}} u_{x,i,N} + \boxed{\tfrac{1}{2}} K^{\mathrm{n}}_{\mathrm{axi}} \left(2u_{x,i,N} - u_{x,i-1,N} - u_{x,i+1,N}\right) + K^{\mathrm{s}}_{\mathrm{axi}} \left(u_{x,i,N} - u_{x,i,N-1}\right) \\ \qquad + \tfrac{1}{2} K^{\mathrm{n}}_{\mathrm{diag}} \left(2u_{x,i,N} - u_{x,i-1,N-1} - u_{x,i+1,N-1}\right) + \tfrac{1}{2} K^{\mathrm{n}}_{\mathrm{diag}} \left(2u_{z,i,N} - u_{z,i-1,N-1} - u_{z,i+1,N-1}\right) = F_{x,i,N} \\ -\boxed{\tfrac{1}{2}}\omega^2 m_{\mathrm{b}} u_{z,i,N} + \boxed{\tfrac{1}{2}} K^{\mathrm{s}}_{\mathrm{axi}} \left(2u_{z,i,N} - u_{z,i-1,N} - u_{z,i+1,N}\right) + K^{\mathrm{n}}_{\mathrm{axi}} \left(u_{z,i,N} - u_{z,i,N-1}\right) \\ \qquad + \tfrac{1}{2} K^{\mathrm{n}}_{\mathrm{diag}} \left(2u_{z,i,N} - u_{z,i-1,N-1} - u_{z,i+1,N-1}\right) + \tfrac{1}{2} K^{\mathrm{n}}_{\mathrm{diag}} \left(2u_{x,i,N} - u_{x,i-1,N-1} - u_{x,i+1,N-1}\right) = F_{z,i,N} \end{cases} \tag{A.9}$$

where $F_{x,i,N}$ and $F_{z,i,N}$ are the externally applied forces at the lower boundary. Compared to the work of Suiker et al. [27], the boundary conditions (A.8)-(A.9) differ by a factor $\frac{1}{2}$ in some of the terms, which are marked with a square ($\boxed{\frac{1}{2}}$). These modified boundary conditions assure that there is no reflection of waves at the interface between two lattice layers with the same properties.

For external forces of the type

$$\begin{bmatrix} F_{x,i,0} \\ F_{\mathrm{z},i,0} \\ F_{x,i,N} \\ F_{\mathrm{z},i,N} \end{bmatrix} = \begin{bmatrix} F_{x,0} \\ F_{\mathrm{z},0} \\ F_{x,N} \\ F_{\mathrm{z},N} \end{bmatrix} \mathrm{e}^{-\mathrm{i}\,\kappa\, id} \tag{A.10}$$

the response of the lattice is as defined in Eq. (A.7). After inserting the solution (A.7) and forces (A.10) into Eqs. (A.8)-(A.9), one obtains

$$\underbrace{\begin{bmatrix}\begin{bmatrix}\mathbf{s}_1\end{bmatrix}\begin{bmatrix}\mathbf{s}_2\end{bmatrix}\begin{bmatrix}\mathbf{s}_3\end{bmatrix}\begin{bmatrix}\mathbf{s}_4\end{bmatrix}\end{bmatrix}}_{\mathbf{S}}\begin{bmatrix}A_1\\A_2\\A_3\\A_4\end{bmatrix}=\begin{bmatrix}F_{x,0}\\F_{z,0}\\F_{x,N}\\F_{z,N}\end{bmatrix} \tag{A.11}$$

where the 4×1 vectors $\mathbf{s}_j$ composing matrix $\mathbf{S}$ are defined as

$$\mathbf{s}_l=\begin{bmatrix}s_{11}&s_{12}&0&0\\s_{21}&s_{22}&0&0\\0&0&s_{33}&s_{34}\\0&0&s_{43}&s_{44}\end{bmatrix}\begin{bmatrix}A_{xl}\\A_{zl}\\A_{xl}\mathrm{e}^{-\mathrm{i}d\kappa_{zl}N}\\A_{zl}\mathrm{e}^{-\mathrm{i}d\kappa_{zl}N}\end{bmatrix} \tag{A.12}$$

The components of the matrix in Eq. (A.12) are as follows:

$$\begin{aligned}
s_{11}&=-\tfrac{1}{2}\omega^2m_\mathrm{b}+K^\mathrm{n}_\mathrm{axi}\left(\tfrac{3}{2}-\cos\left(\kappa d\right)\right)+K^\mathrm{s}_\mathrm{axi}\left(\tfrac{1}{2}-\mathrm{e}^{-\mathrm{i}d\kappa_{zl}}\right)-\tfrac{1}{2}K^\mathrm{n}_\mathrm{diag}\left(\mathrm{e}^{-\mathrm{i}d\left(-\kappa+\kappa_{zj}\right)}+\mathrm{e}^{-\mathrm{i}d\left(\kappa+\kappa_{zl}\right)}\right)\\
s_{12}&=s_{21}=-\tfrac{1}{2}K^\mathrm{n}_\mathrm{diag}\left(\mathrm{e}^{-\mathrm{i}d\left(-\kappa+\kappa_{zl}\right)}-\mathrm{e}^{-\mathrm{i}d\left(\kappa+\kappa_{zl}\right)}\right)\\
s_{22}&=-\tfrac{1}{2}\omega^2m_\mathrm{b}+K^\mathrm{s}_\mathrm{axi}\left(\tfrac{1}{2}-\cos\left(\kappa d\right)\right)+K^\mathrm{n}_\mathrm{axi}\left(\tfrac{3}{2}-\mathrm{e}^{-\mathrm{i}d\kappa_{zl}}\right)-\tfrac{1}{2}K^\mathrm{n}_\mathrm{diag}\left(\mathrm{e}^{-\mathrm{i}d\left(-\kappa+\kappa_{zl}\right)}+\mathrm{e}^{-\mathrm{i}d\left(\kappa+\kappa_{zl}\right)}\right)\\
s_{33}&=-\tfrac{1}{2}\omega^2m_\mathrm{b}+K^\mathrm{n}_\mathrm{axi}\left(\tfrac{3}{2}-\cos\left(\kappa d\right)\right)+K^\mathrm{s}_\mathrm{axi}\left(\tfrac{1}{2}-\mathrm{e}^{\mathrm{i}d\kappa_{zl}}\right)-\tfrac{1}{2}K^\mathrm{n}_\mathrm{diag}\left(\mathrm{e}^{-\mathrm{i}d\left(-\kappa-\kappa_{zj}\right)}+\mathrm{e}^{-\mathrm{i}d\left(\kappa-\kappa_{zl}\right)}\right)\\
s_{34}&=s_{43}=\tfrac{1}{2}K^\mathrm{n}_\mathrm{diag}\left(\mathrm{e}^{-\mathrm{i}d\left(-\kappa-\kappa_{zl}\right)}-\mathrm{e}^{-\mathrm{i}d\left(\kappa-\kappa_{zl}\right)}\right)\\
s_{44}&=-\tfrac{1}{2}\omega^2m_\mathrm{b}+K^\mathrm{s}_\mathrm{axi}\left(\tfrac{1}{2}-\cos\left(\kappa d\right)\right)+K^\mathrm{n}_\mathrm{axi}\left(\tfrac{3}{2}-\mathrm{e}^{\mathrm{i}d\kappa_{zl}}\right)-\tfrac{1}{2}K^\mathrm{n}_\mathrm{diag}\left(\mathrm{e}^{-\mathrm{i}d\left(-\kappa-\kappa_{zl}\right)}+\mathrm{e}^{-\mathrm{i}d\left(\kappa-\kappa_{zl}\right)}\right)
\end{aligned} \tag{A.13}$$

A.3 – Layer stiffness matrix and layered lattices

Similarly to the forces, the displacements at the upper surface ($u_{x,i,0}$ and $u_{z,i,0}$) and those of the lower surface ($u_{x,i,N}$ and $u_{z,i,N}$) can be written as

$$\begin{bmatrix}u_{x,i,0}\\u_{z,i,0}\\u_{x,i,N}\\u_{z,i,N}\end{bmatrix}=\begin{bmatrix}u_{x,0}\\u_{z,0}\\u_{x,N}\\u_{z,N}\end{bmatrix}\mathrm{e}^{-\mathrm{i}\,\kappa\,id} \tag{A.14}$$

where

$$\begin{bmatrix}u_{x,0}\\u_{z,0}\\u_{x,N}\\u_{z,N}\end{bmatrix}=\underbrace{\begin{bmatrix}A_{x1}&A_{x2}&A_{x3}&A_{x4}\\A_{z1}&A_{z2}&A_{z3}&A_{z4}\\A_{x1}e^{-\mathrm{i}d\kappa_{z1}N}&A_{x2}e^{-\mathrm{i}d\kappa_{z2}N}&A_{x3}e^{-\mathrm{i}d\kappa_{z3}N}&A_{x4}e^{-\mathrm{i}d\kappa_{z4}N}\\A_{z1}e^{-\mathrm{i}d\kappa_{z1}N}&A_{z2}e^{-\mathrm{i}d\kappa_{z2}N}&A_{z3}e^{-\mathrm{i}d\kappa_{z3}N}&A_{z4}e^{-\mathrm{i}d\kappa_{z4}N}\end{bmatrix}}_{\mathbf{U}}\begin{bmatrix}A_1\\A_2\\A_3\\A_4\end{bmatrix} \tag{A.15}$$

Eqs. (A.11) and (A.15) can be combined in order to eliminate the unknown modal amplitudes A_l and to obtain a direct relation between forces applied at the upper and lower surfaces and corresponding displacements. This results in

$$\underbrace{\left(\mathbf{S}\,\mathbf{U}^{-1}\right)}_{\mathbf{K}}\begin{bmatrix} u_{x,0} \\ u_{z,0} \\ u_{x,N} \\ u_{z,N} \end{bmatrix} = \begin{bmatrix} F_{x,0} \\ F_{z,0} \\ F_{x,N} \\ F_{z,N} \end{bmatrix} \tag{A.16}$$

The stiffness matrix defined in Eq. (A.16) as $\mathbf{K} = \mathbf{S}\,\mathbf{U}^{-1}$ is very useful in the sense that it allows to consider layered lattices in a straightforward manner. For that, it suffices to calculate the matrices $\mathbf{K}$ for each layer and assemble them in a global matrix in the same fashion as done in the Finite Element Method or in the more similar Stiffness Matrix Method [33]. The resulting global stiffness matrix can then be inverted and multiplied by the external forces acting on the layer interfaces, and by that the displacements of any surface/interface are obtained in the frequency-wavenumber domain. These are the displacements $\overline{u}^{*}_{\alpha\beta,p,q}\left(\kappa\right)$ to which Section 2 refers. For displacements/loads inside the lattice layers, the best approach is to subdivide the layer into several sublayers, with interfaces at the elevations where displacements are required and forces are applied.

A.4 – Semi-infinite lattice layer

In some cases, it may be useful to consider the last layer of the layered lattice with infinite thickness. That is the case when, for example, lattices are used to describe a layered soil whose bed rock is very deep. When this is the case, the procedure to calculate the stiffness matrix changes slightly so that the radiation condition at infinity is considered.

Note that in Eq. (A.5) the vertical eigenvalues κ_{zl} of the lattice come in symmetric pairs, i.e., $\kappa_{z3} = -\kappa_{z1}$ and $\kappa_{z4} = -\kappa_{z2}$. For real eigenvalues, the positive one represents a wave that is propagating downwards while the negative represents a wave propagating upwards. On the other hand, for complex valued eigenvalues, the one with negative imaginary component represents a wave that decays downwards while its counterpart represents a wave decaying upwards. Only the eigenvalue of each pair that respects the radiation condition (wave propagating away from the surface, if eigenvalue is real) or decaying condition (decaying away from the surface, if eigenvalue is complex) is to be used. Thus, for a lower half-space, the stiffness matrix is calculated with

$$\mathbf{K}_{\text{lhs}} = \left[\begin{bmatrix} \\ \mathbf{s}^{\text{lhs}}_{(1|3)} \\ \\ \end{bmatrix}\begin{bmatrix} \\ \mathbf{s}^{\text{lhs}}_{(2|4)} \\ \\ \end{bmatrix}\right]\begin{bmatrix} A_{x(1|3)} & A_{x(2|4)} \\ A_{z(1|3)} & A_{z(2|4)} \end{bmatrix}^{-1} \tag{A.17}$$

where the 2×1 vectors $\mathbf{s}^{\text{lhs}}_{(a|b)}$ are obtained with

$$\begin{bmatrix} \\ \mathbf{s}^{\text{lhs}}_{(a|b)} \\ \\ \end{bmatrix} = \begin{bmatrix} s_{11} & s_{12} \\ s_{21} & s_{22} \end{bmatrix} \begin{bmatrix} A_{x(a|b)} \\ A_{z(a|b)} \end{bmatrix} \tag{A.18}$$

The index pair $(a\,|\,b)$, where $a = 1,2$ and $b = 3,4$ represents the eigenvalue index of the pair κ_{za}, κ_{zb} that is real and positive or that is complex valued with negative imaginary component. The expressions for s_{ij} are given in Eq. (A.13) and are calculated for the eigenvalue κ_{za} or κ_{zb} that fulfils the mentioned conditions.

It is less often the case that a upper half-space is considered. Nevertheless, its stiffness matrix is calculated with

$$\mathbf{K}_{\text{uhs}} = \begin{bmatrix} \begin{bmatrix} \\ \mathbf{s}^{\text{uhs}}_{(1|3)} \\ \\ \end{bmatrix} \begin{bmatrix} \\ \mathbf{s}^{\text{uhs}}_{(2|4)} \\ \\ \end{bmatrix} \end{bmatrix} \begin{bmatrix} A_{x(1|3)} & A_{x(2|4)} \\ A_{z(1|3)} & A_{z(2|4)} \end{bmatrix}^{-1} \tag{A.19}$$

where the 2×1 vectors $\mathbf{s}^{\text{uhs}}_{(a|b)}$ are obtained with

$$\begin{bmatrix} \\ \mathbf{s}^{\text{uhs}}_{(a|b)} \\ \\ \end{bmatrix} = \begin{bmatrix} s_{33} & s_{34} \\ s_{43} & s_{44} \end{bmatrix} \begin{bmatrix} A_{x(a|b)} \\ A_{z(a|b)} \end{bmatrix} \tag{A.20}$$

Contrary to the lower half-space, the eigenvalues to be used in the upper half-space are the negative ones (if real) or the ones with positive imaginary component (if complex valued).

Appendix B

In this appendix, the identity in Eq. (40) is explained. The integral in (40) is a convolution an thus equals to the inverse Fourier transform of the product of the transforms, i.e.,

$$\begin{aligned} &\int_{-\infty}^{+\infty} \begin{bmatrix} u^*_{\text{rail,F}}(x_l - x_0) & u^*_{\text{rail,M}}(x_l - x_0) \\ \theta^*_{\text{rail,F}}(x_l - x_0) & \theta^*_{\text{rail,M}}(x_l - x_0) \end{bmatrix} \begin{bmatrix} F_{\text{ext}}(x_0) \\ M_{\text{ext}}(x_0) \end{bmatrix} \mathrm{d}x_0 \\ &\qquad = \frac{1}{2\pi} \int_{-\infty}^{+\infty} \begin{bmatrix} \tilde{u}^*_{\text{rail,F}}(\tilde{k}) & \tilde{u}^*_{\text{rail,M}}(\tilde{k}) \\ \tilde{\theta}^*_{\text{rail,F}}(\tilde{k}) & \tilde{\theta}^*_{\text{rail,M}}(\tilde{k}) \end{bmatrix} \begin{bmatrix} \tilde{F}_{\text{ext}}(\tilde{k}) \\ \tilde{M}_{\text{ext}}(\tilde{k}) \end{bmatrix} \mathrm{e}^{-\mathrm{i}\tilde{k}\,x_l} \mathrm{d}\tilde{k} \end{aligned} \tag{B.1}$$

where $\tilde{u}^*_{\text{Rail,F}}(\tilde{k})$, $\tilde{\theta}^*_{\text{Rail,F}}(\tilde{k})$, $\tilde{u}^*_{\text{Rail,M}}(\tilde{k})$, $\tilde{\theta}^*_{\text{Rail,M}}(\tilde{k})$ are the Fourier transforms of $u^*_{\text{rail,F}}(x)$, $\theta^*_{\text{rail,F}}(x)$, $u^*_{\text{rail,M}}(x)$ and $\theta^*_{\text{rail,M}}(x)$:

$$\begin{bmatrix} \tilde{u}^*_{\text{rail,F}}(\tilde{k}) & \tilde{u}^*_{\text{rail,M}}(\tilde{k}) \\ \tilde{\theta}^*_{\text{rail,F}}(\tilde{k}) & \tilde{\theta}^*_{\text{rail,M}}(\tilde{k}) \end{bmatrix} = \frac{1}{EI_{\text{rail}}\tilde{k}^4 - \omega^2 m_{\text{rail}}} \begin{bmatrix} 1 & \mathrm{i}\tilde{k} \\ -\mathrm{i}\tilde{k} & -\tilde{k}^2 \end{bmatrix} \tag{B.2}$$

and where $\tilde{F}_{\text{ext}}\left(\tilde{k}\right)$ is

$$\begin{bmatrix} \tilde{F}_{\text{ext}}\left(\tilde{k}\right) \\ \tilde{M}_{\text{ext}}\left(\tilde{k}\right) \end{bmatrix} = \int_{-\infty}^{+\infty} \begin{bmatrix} F_{\text{ext}}\left(x\right) \\ M_{\text{ext}}\left(x\right) \end{bmatrix} \mathrm{e}^{\mathrm{i}\tilde{k}x} \mathrm{d}x = \frac{1}{V} \begin{bmatrix} F_0 \\ M_0 \end{bmatrix} \int_{-\infty}^{+\infty} \mathrm{e}^{\mathrm{i}\left(\omega_0-\omega\right)\frac{x}{V}} \mathrm{e}^{\mathrm{i}\tilde{k}x} \mathrm{d}x = \frac{2\pi}{V} \delta\left(\tilde{k}-\tfrac{\omega-\omega_0}{V}\right) \begin{bmatrix} F_0 \\ M_0 \end{bmatrix} \tag{B.3}$$

Insertion of equalities (B.2) and (B.3) in the second integral of Eq. (B.1) results in

$$\begin{aligned} &\int_{-\infty}^{+\infty} \begin{bmatrix} u^*_{\text{Rail,F}}\left(x_l-x_0\right) & u^*_{\text{Rail,M}}\left(x_l-x_0\right) \\ \theta^*_{\text{Rail,F}}\left(x_l-x_0\right) & \theta^*_{\text{Rail,M}}\left(x_l-x_0\right) \end{bmatrix} \begin{bmatrix} F_{\text{ext}}\left(x_0\right) \\ M_{\text{ext}}\left(x_0\right) \end{bmatrix} \mathrm{d}x_0 = \\ &\qquad \frac{1}{V} \int_{-\infty}^{+\infty} \frac{\delta\left(\tilde{k}-\frac{\omega-\omega_0}{V}\right)}{EI_{\text{rail}}\,\tilde{k}^4-\omega^2 m_{\text{rail}}} \begin{bmatrix} 1 & \mathrm{i}\tilde{k} \\ -\mathrm{i}\tilde{k} & -\tilde{k}^2 \end{bmatrix} \mathrm{e}^{-\mathrm{i}\tilde{k}\,x_l} \mathrm{d}\tilde{k} \begin{bmatrix} F_0 \\ M_0 \end{bmatrix} = \\ &\qquad\qquad \frac{\mathrm{e}^{-\mathrm{i}\frac{\omega-\omega_0}{V}x_l}}{V\left[\left(\frac{\omega-\omega_0}{V}\right)^4 EI_{\text{rail}}-\omega^2 m_{\text{rail}}\right]} \begin{bmatrix} 1 & \mathrm{i}\frac{\omega-\omega_0}{V} \\ -\mathrm{i}\frac{\omega-\omega_0}{V} & -\left(\frac{\omega-\omega_0}{V}\right)^2 \end{bmatrix} \begin{bmatrix} F_0 \\ M_0 \end{bmatrix} \end{aligned} \tag{B.4}$$

This is the identity shown in Eq. (40) of the paper.

References

[1] T. and Dahlberg, Railway Track Stiffness Variations – Consequences and Countermeasures, Int. J. Civ. Eng. 8 (2010). http://ijce.iust.ac.ir/article-1-420-en.html.

[2] D. Li, D. Davis, Transition of railroad bridge approaches, J. Geotech. Geoenvironmental Eng. 131 (2005) 1392–1398.

[3] B. Zuada Coelho, J. Priest, P. Hölscher, Dynamic behaviour of transition zones in soft soils during regular train traffic, Proc. Inst. Mech. Eng. Part F J. Rail Rapid Transit. 232 (2018) 645–662.

[4] A.B. Faragau, A.V. Metrikine, K.N. van Dalen, Transition radiation in a piecewise linear and infinite one-dimensional structure - a Laplace transform method, Nonlinear Dyn. (, submitted).

[5] E. Arlaud, S. COSTA D'AGUAR, E. Balmès, G. Faussurier, Numerical study of railway track dynamics: Case of a transition zone, in: Italy, 2016.

[6] A. Paixão, E. Fortunato, R. Calçada, Transition zones to railway bridges: track measurements and numerical modelling, Eng. Struct. 80 (2014) 435–443.

[7] M. Germonpré, G. Degrande, G. Lombaert, A track model for railway-induced ground vibration resulting from a transition zone, Proc. Inst. Mech. Eng. Part F J. Rail Rapid Transit. 232 (2018) 1703–1717.

[8] B. Indraratna, S. Nimbalkar, D. Christie, The performance of rail track incorporating the effects of ballast breakage, confining pressure and geosynthetic reinforcement, in: Taylor and Francis Group, London, UK, 2009: pp. 5–24.

[9] J. Sae Siew, O. Mirza, S. Kaewunruen, Nonlinear finite element modelling of railway turnout system considering bearer/sleeper-ballast interaction, J. Struct. 2015 (2015).

[10] G. McDowell, O. Harireche, H. Konietzky, S. Brown, N. Thom, Discrete element modelling of geogrid-reinforced aggregates, Proc. Inst. Civ. Eng.-Geotech. Eng. 159 (2006) 35–48.

[11] A. Karrech, D. Duhamel, G. Bonnet, J.-N. Roux, F. Chevoir, J. Canou, J. Dupla, K. Sab, A computational procedure for the prediction of settlement in granular materials under cyclic loading, Comput. Methods Appl. Mech. Eng. 197 (2007) 80–94.

[12] M. Lu, G. McDowell, The importance of modelling ballast particle shape in the discrete element method, Granul. Matter. 9 (2007) 69.
[13] E. Tutumluer, Y. Qian, Y.M. Hashash, J. Ghaboussi, D.D. Davis, Discrete element modelling of ballasted track deformation behaviour, Int. J. Rail Transp. 1 (2013) 57–73.
[14] C. Chen, G.R. McDowell, An investigation of the dynamic behaviour of track transition zones using discrete element modelling, Proc. Inst. Mech. Eng. Part F J. Rail Rapid Transit. 230 (2016) 117–128.
[15] D.G. Duffy, The response of an infinite railroad track to a moving, vibrating mass, J. Appl. Mech. 57 (1990) 66–73.
[16] L. Jezequel, Response of periodic systems to a moving load, J. Appl. Mech. 48 (1981) 613–618.
[17] C. Cai, Y. Cheung, H. Chan, Dynamic response of infinite continuous beams subjected to a moving force—an exact method, J. Sound Vib. 123 (1988) 461–472.
[18] P. Belotserkovskiy, On the oscillations of infinite periodic beams subjected to a moving concentrated force, J. Sound Vib. 193 (1996) 705–712.
[19] T. Hoang, D. Duhamel, G. Forêt, H.P. Yin, P. Joyez, R. Caby, Calculation of force distribution for a periodically supported beam subjected to moving loads, J. Sound Vib. 388 (2017) 327–338.
[20] A. Nordborg, Vertical rail vibrations: Pointforce excitation, Acta Acust. United Acust. 84 (1998) 280–288.
[21] A. Nordborg, Vertical rail vibrations: Parametric excitation, Acta Acust. United Acust. 84 (1998) 289–300.
[22] A. Metrikine, K. Popp, Vibration of a periodically supported beam on an elastic half-space, Eur. J. Mech.-ASolids. 18 (1999) 679–701.
[23] A. Vostroukhov, A. Metrikine, Periodically supported beam on a visco-elastic layer as a model for dynamic analysis of a high-speed railway track, Int. J. Solids Struct. 40 (2003) 5723–5752.
[24] X. Sheng, C. Jones, D. Thompson, Responses of infinite periodic structures to moving or stationary harmonic loads, J. Sound Vib. 282 (2005) 125–149.
[25] D. Clouteau, M. Elhabre, D. Aubry, Periodic BEM and FEM-BEM coupling, Comput. Mech. 25 (2000) 567–577.
[26] A. Suiker, A. Metrikine, R. De Borst, Dynamic behaviour of a layer of discrete particles, Part 2: Response to a uniformly moving, harmonically vibrating load, J. Sound Vib. 240 (2001) 19–39.
[27] A. Suiker, A. Metrikine, R. De Borst, Dynamic behaviour of a layer of discrete particles, Part 1: Analysis of body waves and eigenmodes, J. Sound Vib. 240 (2001) 1–18.
[28] K.F. Graff, Wave Motion in Elastic Solids., Dover Publications, 2012. http://public.eblib.com/choice/publicfullrecord.aspx?p=1894353.
[29] M. Corinthios, Signals, systems, transforms, and digital signal processing with MATLAB, CRC Press, 2009.
[30] Wolfram|Alpha (www.wolframalpha.com, accessed on 15-11-2018), n.d. www.wolframalpha.com.
[31] L. Brillouin, Wave propagation in periodic structures : electric filters and crystal lattices, McGraw-Hill, New York [etc.], 1946.
[32] A. Suiker, A. Metrikine, R. De Borst, Comparison of wave propagation characteristics of the Cosserat continuum model and corresponding discrete lattice models, Int. J. Solids Struct. 38 (2001) 1563–1583.
[33] E. Kausel, J.M. Roesset, Stiffness matrices for layered soils, Bull. Seismol. Soc. Am. 71 (1981) 1743–1761.